Coastal Eddies as Vectors for Connectivity During the Summer in the Levantine Sea

Yotam Fadida[1,2], Tal Ozer[1], Tal Ben Ezra[3], Michael D. Krom[3,4], Anat Tsemel[3], Tatiana Margo Tsagaraki[5], Eli Biton[1], Yaron Toledo[6], and Yoav Lehahn[2]

[1]Israel Oceanographic and Limnological Research, Haifa, Israel
[2]Department of Marine Geosciences, Leon H. Charney School of Marine Sciences, University of Haifa, Haifa, Israel
[3]Morris Kahn Marine Research Station, Department of Marine Biology, Leon H. Charney School of Marine Sciences, University of Haifa, Haifa, Israel
[4]School of Earth and Environment, University of Leeds, Leeds, UK
[5]Department of Biological Sciences, University of Bergen, Bergen, Norway
[6]School of Mechanical Engineering, Tel-Aviv University, Tel-Aviv-Yafo, Israel

Correspondence: Yoav Lehahn (ylehahn@univ.haifa.ac.il), Yotam Fadida (yotam@ocean.org.il)

Abstract. The Levantine Basin, the easternmost part of the Mediterranean Sea, is one of the most oligotrophic marine environments worldwide. A pronounced gradient separates its relatively chlorophyll-enriched coastal zone from the severely depleted offshore waters, and the degree of connectivity between these regions shapes the distribution of biomass and nutrients. The connectivity between these two contrasting regimes is highly seasonal: during winter, deep mixing and enhanced lateral stirring promote basin-wide exchange, whereas in summer, strong stratification and a persistent alongshore current largely suppress cross-shore transport. Coastal mesoscale eddies are recurring features along the eastern Levantine margin, yet their subsurface structure and biogeochemical footprint remain poorly characterized. Here, we use an event-based approach focusing on three coastal eddy events, combining satellite imagery, autonomous glider transects, high-frequency (HF) radar measurements, and cruise-based profiles to examine their three-dimensional structure and role in summertime coastal–offshore exchange. ~~Here, we combine satellite imagery, autonomous glider transects, high-frequency (HF) radar measurements, and cruise-based profiles to examine the three-dimensional structure of these eddies and their role in summertime coastal–offshore exchange.~~[R1] Glider observations reveal a distinct vertical signature within the eddies, with warmer coastal-origin waters and a shoaling of the deep chlorophyll maximum (DCM) from approximately 120–130 m in surrounding offshore waters to approximately 50 m within the eddies. Cruise profiles reveal elevated subsurface concentrations of silica and inorganic particulate matter. HF radar measurements document anticyclonic circulation and offshore propagation of the coastal eddies. ~~Independent cruise observations further show elevated silica and inorganic particulate matter concentrations extending below the surface, while HF radar measurements reveal dynamically coherent anticyclonic circulation within the coastal mesoscale eddies and their offshore propagation.~~[R1] Together, these multi-platform observations demonstrate that coastal mesoscale eddies are three-dimensional transport features that temporarily breach the summertime coastal–offshore barrier, carrying a distinct~~coherent~~[R2] physical and biogeochemical coastal water-mass signature into one of the world's most oligotrophic marine regions.

1 Introduction

The Eastern Mediterranean Sea (EMS), particularly its easternmost sub-basin, the Levantine Basin, is among the most oligotrophic marine environments on Earth (Krom et al., 2005, 2014; Psarra et al., 2000). Extremely low concentrations of macronutrients, particularly phosphate, nitrate, and silicate, and correspondingly low primary productivity are defining characteristics of its offshore waters (Kress and Herut, 2001; Moutin et al., 2012; Pujo-Pay et al., 2011). Within this generally nutrient-depleted setting, a cross-shore gradient exists between the coastal region—where sediment-water interactions and terrestrial inputs can moderately enhance nutrient availability, chlorophyll concentrations, and primary production (Azov, 1986; Berman et al., 1984; Nixon, 2003; Krom et al., 2004; Kress and Herut, 1998; Raveh et al., 2015; Herut et al., 1999)—and the ultra-oligotrophic offshore waters (Crombet et al., 2011; Zohary and Robarts, 1998; Ignatiades et al., 2009). Although this contrast is weaker than in other coastal–offshore systems, including more productive regions of the Mediterranean Sea and stratified marginal seas influenced by stronger terrestrial inputs (Ben-Ezra et al., 2023; Solidoro et al., 2009; Powley et al., 2017; Han et al., 2012), it remains an important element of the ecological structure of the Levantine Basin (Reich et al., 2022; Herut et al., 2000; Raveh et al., 2015).

Exchanges between the coastal and offshore domains influence nutrient supply, primary production, and ecosystem functioning across the Levantine Basin (Ribera d'Alcalà et al., 2003; Siokou-Frangou et al., 2010). Periods of enhanced connectivity, reflecting increased coastal–offshore exchange and transport, can redistribute biomass and nutrient-enriched waters offshore (Barale et al., 2008; Alkalay et al., 2020; Katz et al., 2020) whereas reduced connectivity leaves the offshore region relatively isolated. The efficiency and pathways of this coastal–offshore exchange, therefore, play a central role in shaping regional biogeochemical variability.

Connectivity in the EMS exhibits strong seasonality (Estrada, 1996; Rosentraub and Brenner, 2007). During winter, vertical mixing deepens the mixed layer and injects nutrients into the euphotic zone (Siokou-Frangou et al., 2010; Barale et al., 2008), while submesoscale (typically ∼1–10 km) instabilities enhance lateral stirring (Lévy et al., 2012). Recent work indicates that such wintertime horizontal processes contribute substantially to the seasonal offshore chlorophyll increase (Fadida et al., 2026). These findings emphasize the role of submesoscale (∼1–10 km) and mesoscale (∼10–100 km) processes in regulating offshore enrichment during the winter.

In contrast, during the more stratified summer conditions, the connectivity regime changes markedly. Strong stratification suppresses vertical nutrient resupply, while the persistent alongshore current limits cross-shore exchanges, effectively decoupling the coastal zone from the offshore basin (Ozer et al., 2022; Verma et al., 2024; Akpınar, 2024). As a result, offshore waters remain extremely nutrient-poor, and coastal signals are typically confined nearshore. As such, any mechanisms capable of intermittently bridging the coastal–offshore divide during summer are of particular interest, even if their overall contribution is episodic or spatially limited.

Mesoscale eddies are rotating structures with characteristic sizes related to the local first baroclinic Rossby radius of deformation[R1] (Chelton et al., 1998). This radius typically ranges from 5 to 15 km across the Mediterranean, with smaller values over continental shelves[R1] (Kurkin et al., 2020), and is approximately 12 km in the eastern Mediterranean[R1] (Amitai

et al., 2010). Eddy diameters can be several times larger, with values of approximately 40–80 km reported in the Levantine Basin[R1] (Robinson et al., 2001). Their associated sea-surface height (SSH) anomalies, generally positive for anticyclones and negative for cyclones, provide a widely used indicator of geostrophic circulation in large open-ocean eddies[R1] (Dufau et al., 2016; Amitai et al., 2010; Pegliasco et al., 2021). Previous studies in the Mediterranean have characterized large anticyclonic eddies using hydrographic observations, cruise measurements, drifters, and SSH-based analyses, focusing on their circulation, persistence, and physical structure[R1] (Zodiatis et al., 2023; Moutin et al., 2012; Barboni et al., 2021; Poulain et al., 2013). These include eddies with diameters of approximately 60–130 km in the Algerian Basin, whose spatial scales are more readily captured by gridded altimetry products[R1] (Pessini et al., 2018, 2020; Cotroneo et al., 2016).

More recently, regional numerical models have achieved sufficiently high spatial resolution to resolve smaller coastal mesoscale eddies and their interaction with the Levantine boundary current[R1] (Verma et al., 2024; Solodoch et al., 2023). Observational characterization of these features remains challenging, however. The coastal eddies investigated here typically have diameters of 30–40 km and develop immediately adjacent to the coastline. Although the DUACS gridded altimetry product has a nominal grid spacing of 0.0625° (∼7 km), its effective resolving capability is coarser, limiting the characterization of these small coastal eddies. Coastal proximity introduces additional uncertainties associated with land contamination and interpolation[R1] (Birol et al., 2025). Ocean-colour imagery offers a complementary means of delineating these features by tracing chlorophyll-rich coastal waters extending offshore. Accordingly, this study combines satellite chlorophyll fields for eddy identification with HF-radar observations to assess circulation and propagation. [R1]

Along the Levantine coast, coastal mesoscale eddies are frequently observed during summer (Menna et al., 2012; Estournel et al., 2021; Efrati et al., 2013). Their formation has been attributed to wind-driven current separation, mesoscale instabilities, and bathymetric deflection of the coastal jet, as documented by high-resolution models, in situ observations, and satellite analyses (Akpınar, 2024; Gerin et al., 2009; Verma et al., 2024; Baaklini et al., 2024). While these structures are known to extend offshore and advect surface tracers (Gertman et al., 2010; Martin, 2003; Flos and Tintoré, 1990), their role in coastal–offshore exchange under summer stratification remains uncertain. During this season, the Levantine Basin is characterized by strong vertical stratification, extremely low surface nutrient concentrations, and a pronounced DCM (the subsurface layer characterized by a local maximum in chlorophyll-a concentration[R2]) near the nutricline (Mignot et al., 2014; Teruzzi et al., 2021; Ediger and Yilmaz, 1996; Ben-Ezra et al., 2024). Global BGC-Argo analyses show that mesoscale eddies modify DCM characteristics in stratified waters[R1] (Cornec et al., 2021). Regional studies further demonstrate eddy-related changes in subsurface chlorophyll maxima and nutrient availability in the South China Sea[R1] (Xu et al., 2023), and in shelf chlorophyll distributions under strong seasonal stratification adjacent to the East Australian Current[R1] (Malan et al., 2023). ~~In other stratified coastal systems, mesoscale eddies have been shown to reorganize surface chlorophyll, DCM, and the nutrient field under stratified conditions.~~[R1]

Although surface chlorophyll anomalies associated with coastal eddies in the Levantine Basin have previously been documented using satellite and in situ observations (Efrati et al., 2013; Baaklini et al., 2024), observations of their subsurface structure remain limited, particularly below the surface mixed layer.~~these studies were limited to the surface expression of the eddies, and no characterization of their three-dimensional water-column structure has been reported for this region.~~[R1]

In this study, we investigate the role of coastal mesoscale eddies as episodic pathways for summer cross-shelf exchange in the eastern Levantine Basin by characterizing their three-dimensional physical and biogeochemical structure. Combining satellite-derived chlorophyll fields, HF radar surface currents, autonomous glider transects, and ship-based nutrient, major element particulate matter geochemistry and chlorophyll profiles, we identify ~~coherent~~ [R2] coastal eddies and quantify their propagation and kinematics. Since the offshore transport investigated here occurs through intermittent mesoscale events rather than persistent background exchange, an event-scale approach was adopted (McNeil et al., 1999; Holte et al., 2013; Li et al., 2008). Such transient features can produce substantial local transport despite their episodic occurrence (Rubio et al., 2018; Feng, 2009; Chenillat et al., 2015) and may therefore not be adequately captured by seasonal or climatological averaging. Our results demonstrate that coastal mesoscale eddies can intermittently breach the summertime coastal–offshore barrier in the Levantine Basin, transporting a distinct coastal physical and biogeochemical water-mass signature below the surface mixed layer into one of the world's most oligotrophic marine regions. ~~Our results provide the first observational evidence that coastal mesoscale eddies can intermittently breach the summertime coastal–offshore barrier, transporting a coherent coastal physical and biogeochemical water-mass signature into one of the world's most oligotrophic marine regions.~~ [R2]

2 Data and Methods

2.1 Data

2.1.1 Satellite data.

This study was conducted using E.U. Copernicus Marine Service Information. Initial identification and selection of the investigated transport events were performed using L3 satellite observations (DOI: 10.48670/moi-00299), and only cases with clearly visible transport structures were retained. L4 (DOI: 10.48670/moi-00300) products were subsequently used for visualization and presentation of continuous spatial fields. A quantitative comparison between the L3 and L4 products is provided in Tables A1 and A2, while Figs. A1 and A2 present side-by-side comparisons of the corresponding figures. These comparisons demonstrate that the interpolation applied in the L4 products has a negligible influence on the detected eddy geometry and the quantitative metrics used in this study. Estimation of the mass concentration of chlorophyll-a in seawater (CHL) was derived from the gridded L4 daily ocean-color (1/100 degrees spatial resolution) data set. Data from several satellite missions (SeaWiFS, MODIS, MERIS, VIIRS-SNPP and JPSS1, OLCI-S3A) are combined to provide interpolated gap-free data sets (Volpe et al., 2018), using region-specific algorithms (Case-1 waters (Volpe et al., 2019), with new coefficients; and Case-2 waters (Berthon and Zibordi, 2004)). The images were all taken approximately at 13:00, which is generally when the satellite passes over the region.

Absolute dynamic topography (ADT) and associated surface geostrophic currents were obtained from the Copernicus Marine reprocessed European Seas Level-4 product (DOI: 10.48670/moi-00141), provided daily on a grid with a spacing of 1/16 degrees.

Sea Surface Temperature (SST) was estimated with the Copernicus Ultra High Resolution Sea Surface Temperature Analysis

L4 product DOI: doi.org/10.48670/moi-00172, with a spatial resolution of 1/100 degrees.

Satellite chlorophyll data were analyzed for all observational periods, including the June–July 2018 (M141) and June–July 2022 (M164) glider missions, the 30 July–3 August 2020 HF-radar observations, and the *N800* cruise sampling events on 30 July and 15 September 2020. SST data were analyzed for the two glider missions and to provide regional context (30 July 2020). Geostrophic currents derived from ADT were used solely to provide regional circulation context for the 30 July 2020 event.

2.1.2 High Frequency Radar

The Israeli coastal HF-radar network, operated by the Marine Engineering and Physics Laboratory at Tel Aviv University, consists of two WERA (WavE Radar; Gurgel et al. (1999)) systems located at Ashkelon and Ashdod along the southeastern Mediterranean coast (Lorente et al., 2022). Each station operates in a monostatic configuration with co-located transmit and 12-element receive arrays, transmitting at a central frequency of 8.3 MHz and providing radial current coverage of up to approximately 180 km, depending on environmental conditions (Crombie, 1955; Barrick, 1977; Wyatt, 1991). The two sites are separated by roughly 25-km to optimize the overlap of their radial coverage for wave measurements (Hasselmann, 1971; Gurgel et al., 2006). This relatively close spacing ensures sufficiently large crossing angles between the two radar beams in the near field, improving the conditioning of directional inversions and enhancing the reliability of derived wave spectra. At the same time, the configuration constrains the region of robust two-dimensional current and wave mapping to about 75-km offshore, beyond which geometric dilution and weaker second-order backscatter reduce retrieval accuracy. The underlying radial measurements had a range resolution of approximately 300–750 m and a nominal angular spacing of 1°, with effective beamforming-related azimuthal averaging increasing from approximately $\pm 4^\circ$ near the center of the coverage to $\pm 8^\circ$ near its edges. Surface-current maps were interpolated onto a nominal x–y grid with approximately 1.4 km spacing. The current measurement dataset is related to continuous measurements conducted between July 30th and August 3rd 2020. Each radar was operating in 20-minute measurement cycles consisting of approximately three minutes of passive listening, used to identify a clean frequency band, followed by 17 minutes of active data acquisition. The resulting measurements were averaged to produce three current maps per hour. The analyses presented in this study are based on three-hour averages, corresponding to the mean of nine consecutive 20-minute radial and vector field maps taken to improve accuracy for the flow time-scales of interest. The three-hour average used in the analysis is 12:00-15:00 to coincide with the passage of the satellite over the region.

2.1.3 Glider Data

An autonomous underwater vehicle (SeaExplorer glider, Alseamar) equipped with a fluorometer by WetLabs and a CTD (conductivity, temperature, depth) by Sea-Bird was deployed for a variety of missions between the years 2018-2023. The missions (M141, M164) that coincided with summertime coastal eddies were analyzed for this study. The glider collected CTD and fluorescence data at very high spatiotemporal coverage through the upper 700 m of the water column. 360 dives were utilized from M141's mission between 24 June and 03 July 2018, yielding a 118 km transect (repeated twice). 55 dives were utilized from M164's mission between 29 June and 03 July 2022, yielding an 85 km transect. Glider dives, horizontally spaced

at 3 km intervals, were separated into descending and ascending profiles and treated as quasi-vertical measurements (1.5 km apart).

2.1.4 Cruise Data

N800 cruises — Data were obtained from a pelagic time-series station (*N800*; 32.52° N, 34.72° E) located 15 km offshore of the Israeli coast at a water depth of 832 m. The station was sampled approximately monthly throughout 2020. The results presented here correspond to sampling periods during which coastal mesoscale eddies were observed to pass over the station (30 July 2020 and 15 September 2020), together with routine sampling conducted under non-eddy conditions for comparison. Background variability for dissolved nutrients and particulate constituents was calculated from the non-eddy sampling periods within the stratified season (April–November (D'Ortenzio et al., 2005)), excluding the July and September eddy-influenced sampling periods.

Sampling was conducted from the *R/V Mediterranean Explorer* using a rosette system equipped with 12 Niskin bottles. Hydrographic profiles were obtained with a Sea-Bird Electronics SBE19plusV2 CTD equipped with sensors for conductivity, temperature, fluorescence (used as a proxy for chlorophyll-a; Zeng and Li, 2015), turbidity, photosynthetically active radiation (PAR), and, for selected cruises, dissolved oxygen. Sampling was typically conducted between 10:00 and 13:00 local time, coinciding with satellite overpass of the region.

Particulate Fe, Si, and C (and other major elements) concentrations were measured using thin-film X-ray fluorescence (XRF) at depths of 25, 100, and 180 m (Paulino et al., 2013). Organic matter (OM) and inorganic matter (IM) were estimated from thin-film XRF measurements of organic carbon and Si. OM was calculated as twice the measured organic carbon concentration, while IM was estimated assuming that Si constitutes 20 % of total inorganic particulate matter (Goldsmith et al., 2001).

Detailed descriptions of the sampling procedures and analytical methods for dissolved nutrients and major particulate elements measured by thin-film XRF are provided in Ben-Ezra et al. (2024). Analytical precision and limits of detection for the dissolved nutrient measurements are provided in Table A3.

Haifa Section Cruises — Haifa Section Cruises have been conducted by the *Israeli Oceanographic and Limnological Research Institute* twice a year (summer and winter) since 2002 (54 cruises to date). During these cruises, physical, chemical, and biological data are collected along a transect of eight stations extending from Haifa Bay into the open sea, perpendicular to the Israeli shelf. The chlorophyll measurements used in Fig. A5 represent the average of four summer cruises conducted during August–September of 2018–2021 and are presented to illustrate the typical chlorophyll transect under non-eddy conditions. For detailed cruise sampling and laboratory analysis methods, see Ozer et al. (2017).

2.2 Methods

~~Mesoscale eddies are commonly identified using sea-surface height (SSH) anomalies, as the associated sea-level expression provides a robust indicator of geostrophic circulation for large open-ocean vortices . In the Mediterranean Sea, SSH-based analyses have successfully characterized mesoscale eddies with typical diameters of approximately 60–130 km, including those in the Algerian Basin, where their spatial scales are well resolved by gridded altimetry products. The coastal eddies~~

~~investigated here, however, are substantially smaller. These features typically have diameters of only 30–40 km and develop immediately adjacent to the coastline. Although the DUACS gridded altimetry product has a nominal grid spacing of 0.0625° (~7 km), its effective spatial resolution during the study period was approximately 0.125° (~14 km), meaning that eddies of this size are represented by only a few independent observations, while coastal proximity further increases uncertainty due to land contamination and interpolation . The limited representation of these smaller coastal features in SSH is also evident in Fig. 1, where the coastal eddies are clearly expressed in the chlorophyll field and, to a lesser extent, in SST, whereas only the largest offshore feature is clearly discernible in the SSH field. Ocean-colour imagery directly traces the transport of chlorophyll-rich coastal waters, providing a more suitable observational framework for delineating the offshore extent of these transport events. Consequently, chlorophyll fields were used for eddy identification throughout this study, while HF-radar observations were used to validate the circulation and propagation of the tracked coastal eddies.~~[R1] The following analyses were designed to identify episodic offshore transport events associated with coastal mesoscale activity and characterize their physical and biogeochemical signatures. Two complementary approaches were applied. First, offshore chlorophyll anomalies were identified to estimate the extent of transported coastal waters and associated chlorophyll redistribution. Second, a frontal analysis was applied to characterize the dynamically active boundaries of these features and enable HF-radar collocation and kinematic analysis.

2.2.1 Identification and characterization of coastal mesoscale eddies

The analyses were performed sequentially using satellite chlorophyll images as the primary detection tool. Daily satellite observations were first examined to identify offshore chlorophyll features associated with coastal mesoscale transport. These features were then cross-referenced with the timing and locations of available autonomous glider missions, research cruises, and HF-radar observations to identify events for which complementary physical, biogeochemical, and kinematic measurements were available. Three coincident events were selected for detailed analysis.

Following the event selection, the analyses were performed using the sequential procedure described below. Satellite chlorophyll observations were used to delineate the offshore transport features and quantify their geometry and chlorophyll redistribution, while coincident glider and HF-radar observations were incorporated where available to characterize their three-dimensional structure and surface kinematics, respectively.

Step 1 – Define the offshore analysis domain

An offshore analysis domain was first defined using the 700 m isobath (Fig. 1, dashed black line). Only chlorophyll anomalies located seaward of this contour were considered, because the objective was to identify coastal waters that had been transported beyond the continental shelf and slope into the open Levantine Basin. Along this section of the Levantine coast, the continental margin is narrow and steep, with the transition from the shelf to the deep basin occurring over approximately the 200–1000 m depth range. The 700 m contour therefore provides a representative mid-slope boundary, and small shifts in the selected isobath have limited influence on the detected offshore features because of the steep bathymetric gradient.

Step 2 – Estimate the daily offshore background

The offshore background chlorophyll concentration was calculated independently for each daily map to account for temporal variability in offshore conditions. The background was computed from pixels located seaward of the 700 m isobath within 33.0–35.5°E, 31.0–33.7°N[R2], using the mean chlorophyll concentration between the 20th and 80th percentiles. Restricting the calculation to this percentile range reduced the influence of very low values and localized high-chlorophyll features that could bias the background estimate.

Step 3 – Detect offshore chlorophyll anomalies

A daily detection threshold C_{th} was defined as twice the mean offshore background chlorophyll concentration,

$$C_{\mathrm{th}} = 2\overline{C}_{\mathrm{bg}} \tag{1}$$

where $\overline{C}_{\mathrm{bg}}$ is the mean daily offshore background chlorophyll concentration. This conservative threshold was selected empirically to isolate robust offshore chlorophyll anomalies associated with transported coastal waters while minimizing the inclusion of weak offshore background variability.

Step 4 – Delineate offshore transport features

Contiguous regions exceeding the threshold were identified as individual offshore chlorophyll features (magenta lines in Fig. 2, 3B, 4B). The three events selected for further analysis were those that coincided with independent observations from autonomous gliders, research cruises, or the HF-radar system. The detected features were interpreted as coastal mesoscale eddies on the basis of their spatial continuity~~their coherent geometry~~[R2] and the complementary physical and biogeochemical observations presented in the following. The horizontal surface area of each eddy was calculated by converting the dimensions of the latitude–longitude grid cells into spherical cell areas and summing the area of all pixels contained within the corresponding satellite-derived mask.

Estimation of chlorophyll redistribution

For the two eddies sampled by autonomous gliders (Figs. 3 and 4), satellite-derived surface masks were integrated with glider chlorophyll profiles to estimate the three-dimensional chlorophyll anomaly associated with each eddy (Figs. 5 and 6). Profiles collected seaward of the 700 m isobath and [R2]within the eddy interior, $C_{\mathrm{eddy}}(z)$, were compared with reference profiles, $C_{\mathrm{ref}}(z)$, obtained from adjacent offshore waters outside the eddy (black dotted rectangles in Figs. 3 and 4). A total of 25 eddy and 25 reference profiles were used for the 2018 mission (M141), and 15 eddy and 15 reference profiles for the 2022 mission (M164). The vertical chlorophyll anomaly was defined as

$$\Delta C(z) = C_{\mathrm{eddy}}(z) - C_{\mathrm{ref}}(z) \tag{2}$$

where positive values represent chlorophyll enrichment relative to the offshore reference profile and negative values represent depletion. Both positive and negative contributions were retained in the subsequent integration. The vertically integrated chlorophyll anomaly per unit area ΔC_{int} was then calculated as

$$\Delta C_{\mathrm{int}} = \int_{0}^{z_{\max}} \Delta C(z)\, dz \tag{3}$$

where $z_{\max}$ is the maximum depth over which both the eddy and reference profiles were defined. Finally, the total chlorophyll anomaly associated with each eddy was estimated as

$$\Delta C_{\mathrm{total}} = A_{\mathrm{eddy}}\, \Delta C_{\mathrm{int}} \tag{4}$$

where A_{eddy} is the satellite-derived horizontal surface area of the eddy.

2.2.2 Gradient-based detection of the eddy frontal boundary

For the eddy sampled within the HF-radar observation domain (Fig. 2), the satellite-derived eddy mask obtained in Section 2.2.1 served as the starting point for frontal-boundary detection. Rather than searching the entire chlorophyll field for fronts, the analysis was restricted to the previously detected eddy to isolate its dynamically active transport boundary.

Step 1 – Delineate the offshore eddy

The offshore eddy was first identified using the chlorophyll-anomaly detection procedure described in Section 2.2.1 (magenta outline in Fig. 2).

Step 2 – Calculate chlorophyll gradients

Horizontal chlorophyll gradients were calculated in metric units within the satellite-derived eddy mask. Restricting the analysis to this region excluded unrelated fronts elsewhere in the satellite image.

Step 3 – Identify the frontal boundary

A gradient threshold, G_{th}, was defined as the 90th percentile of the chlorophyll-gradient magnitude within the satellite-derived eddy mask,

$$G_{\mathrm{th}} = P_{90}\left(|\nabla C|_{\mathrm{eddy}}\right) \tag{5}$$

where P_{90} denotes the 90th percentile of chlorophyll-gradient magnitudes within the detected eddy.

Pixels satisfying

$$|\nabla C(\mathbf{x})| \geq G_{\mathrm{th}} \tag{6}$$

were classified as frontal pixels. This criterion isolated the sharp chlorophyll gradient separating the frontal limb from the immediately adjacent offshore background.

Step 4 – Extract the frontal polygon and track eddy propagation

Frontal pixels were grouped into connected regions, and an isocontour was extracted to form a continuous polygon representing the frontal limb of the eddy (shaded magenta region in Fig. 2A-E). Because the eddy propagated predominantly toward the northeast, the northeasternmost pixel of the frontal polygon was used as a representative tracking point. Its position was tracked between consecutive days to determine the eddy's propagation pathway and calculate its propagation velocity (white dot in Fig. 2A-E).

Step 5 – HF-radar collocation and kinematic analysis

The frontal polygon was subsequently collocated with HF-radar surface-current observations (Fig. 2F-J). A manually selected eddy center was used to determine the radial direction at each HF-radar measurement location, and the measured current vectors were projected onto the tangential direction to obtain azimuthal velocities (Fig. A3). Maximum, minimum, and mean azimuthal velocities were calculated from all HF-radar measurements contained within the frontal polygon, providing estimates of the eddy's rotational intensity.

3 Results

3.1 Regional context: summertime mesoscale activity and basin-scale biogeochemical structure

A basin-scale snapshot of summer surface conditions in the Eastern Mediterranean Sea (30 July 2020) reveals a close correspondence between mesoscale circulation and surface chlorophyll distributions (Fig. 1). Offshore anticyclonic features with elevated SSH, such as the Cyprus Eddy (Zodiatis et al., 2023), exhibit low surface chlorophyll concentrations in this snapshot, consistent with strong stratification and suppressed nutrient supply (Krom et al., 1992; Belkin et al., 2022). In contrast, the Rhodes Gyre, a larger-scale cyclonic circulation feature characterized by depressed SSH[R1] (Robinson et al., 1991; Marullo et al., 2003), coincides with locally enhanced surface chlorophyll, consistent with its upwelling-favorable dynamical setting[R1] (van Leeuwen et al., 2022).~~In contrast, cyclonic eddiesidentified by depressed SSH, such as the Rhodes Gyre, coincide with locally enhanced surface chlorophyll, reflecting their upwelling-favorable dynamical setting.~~[R1]

Along the southern Levantine coast, surface chlorophyll concentrations are not uniformly elevated relative to the offshore basin. Instead, enhanced coastal chlorophyll is primarily observed downstream of the Nile River Delta, the dominant source of nutrient-rich coastal waters in the region (Nixon, 2003; El-Rayis and Abdallah, 2006; Oczkowski et al., 2009). This downstream

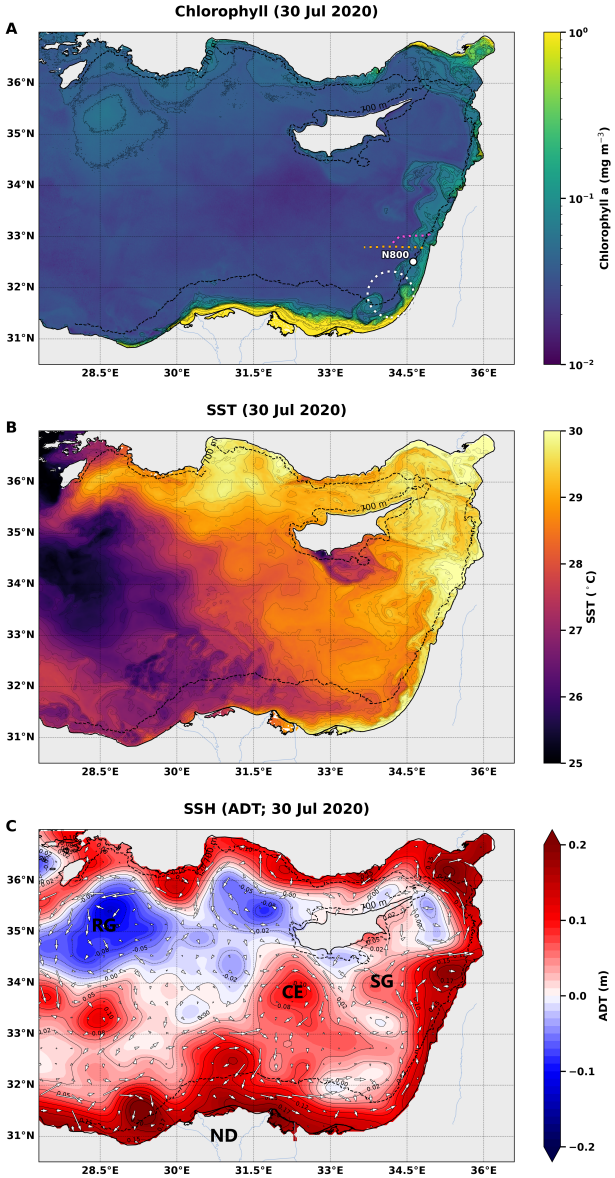

Figure 1. Summer surface conditions in the Eastern Levantine Basin on 30 July 2020. A. Surface chlorophyll (mg m^{-3}), highlighting a sequence of mesoscale eddies extending downstream of the Nile River Delta and progressing cyclonically across the basin. The 700 m isobath is shown as a black dotted line. Dotted amber line shows the glider path on mission M141, magenta line shows the glider path on mission M164. White dot shows location for TS station N800 and white dotted circle shows the coverage region for the HF radar. B. Sea surface temperature (SST) and C. Absolute dynamic topography (ADT) and geostrophic currents derived from satellite altimetry for 30 July 2020. Locations of significant regions such as Rhodes Gyre (RG), Cyprus Eddy (CE), Shikmona Gyre (SG), and the Nile River Delta (ND).

asymmetry is evident in the distribution of coastal mesoscale features: anticyclonic eddies located west of the Nile Delta (upstream) exhibit little to no surface chlorophyll enhancement (Fig. 1A,C - 31.5° N, 28.75° E), whereas anticyclonic eddies east of the Delta (downstream) display pronounced surface chlorophyll signatures (Fig. 1A), (Fadida et al., 2026).

Against this basin-wide background, during summer, a sequence of mesoscale meanders and eddies is embedded in the Levantine along-shore coastal current (Fig. 1A-C). Unlike the offshore anticyclonic features, these downstream coastal eddies exhibit elevated surface chlorophyll concentrations despite their anticyclonic nature. The associated sea surface temperature field (Fig. 1B) further indicates that these features are composed of relatively warm coastal-origin waters that are advected along the shoreline.

The regional snapshot further shows that coastal mesoscale features are dynamically connected to the larger-scale circulation. In particular, one of the downstream coastal eddies is observed to extend offshore and merge with the Shikmona Gyre (33.41° N, 34.25° E). Related processes have been documented in numerical simulations and satellite observations.[R1] Verma et al. (2024) described the formation, propagation, and merging of boundary-current anticyclonic spirals, illustrated through normalized relative vorticity fields, while[R1] Barboni et al. (2021) used SST imagery to document the detachment of a warm-core anticyclonic ring from the Levantine coast and its subsequent merging with offshore anticyclones. The chlorophyll signature shown here suggests a pathway by which Nile-influenced coastal waters can reach the offshore basin.[R1] This basin-scale context highlights coastal eddies as a distinct class of mesoscale features whose biogeochemical signature reflects both their dynamical structure and their upstream conditioning within the coastal boundary current.

3.2 Eddy kinematics and propagation

To determine whether the downstream coastal features identified in Fig. 1 are associated with mesoscale circulation~~represent dynamically coherent mesoscale eddies~~[R2] rather than transient surface tracer patches, we analyzed a series of collocated satellite chlorophyll imagery and HF-radar surface current measurements from 30 July to 3 August 2020 (Fig. 2). We examine whether the HF-radar velocity field exhibits organized anticyclonic rotation and whether rotational velocities exceed the estimated propagation speed, a relationship consistent with potential fluid trapping within the eddy interior ~~Here, we consider the feature dynamically coherent if the HF-radar velocity field exhibits organized anticyclonic rotation around the eddy and rotational velocities exceed the downstream propagation speed, indicating internal circulation rather than passive advection.~~[R2](Chelton et al., 2011). Over five consecutive days, satellite observations captured the downstream evolution of a coastal anticyclonic feature, whose leading northeastern frontal segment advanced seaward along the Levantine coast.

Tracking the displacement of this frontal boundary indicates that the eddy propagated at a mean speed of approximately 0.155 m s^{-1} (∼13.4 km day^{-1}). Concurrent HF-radar measurements reveal a well-defined azimuthal circulation that is spatially collocated with the chlorophyll-defined eddy boundary. Tangential speeds ranged from 0.11–0.36 m s^{-1} on 30 July, 0.30–0.64 m s^{-1} on 31 July, and 0.37–0.73 m s^{-1} on 1 August, 0.14–0.93 m s^{-1} on 2 August, and 0.05–0.67 m s^{-1} on 3 August, with mean values ranging from 0.21 to 0.68 m s^{-1} over the same period. Within the portions of the chlorophyll feature sampled by HF radar, azimuthal velocities are predominantly negative, indicating clockwise, anticyclonic circulation (Fig. A3). This pattern is apparent as the feature moves into the radar domain, although coverage of its circulation varies between days.[R2]

At all stages, mean azimuthal speeds exceeded the estimated mean propagation speed, consistent with substantial rotational motion within the sampled feature.~~the measured azimuthal velocities exceeded the downstream propagation speed by a factor of two to six, indicating that the feature was dominated by rotational motion rather than simple advection by the background flow.~~[R2] ~~The persistence of a closed anticyclonic circulation over multiple days confirms that the observed structure represents a dynamically coherent mesoscale eddy.~~[R2]

3.3 Eddy structure from glider observations

To characterize the three-dimensional structure of coastal mesoscale eddies during summer stratification, we analyzed two independent autonomous glider missions that intersected coastal eddies identified in satellite imagery (Figs. 3 and 4). Although separated by four years (2018 and 2022) and sampling different eddies, both missions revealed remarkably similar vertical physical and biogeochemical structures. Together, these observations demonstrate that coastal mesoscale eddies consistently transport a distinct coastal water-mass signature into the offshore Levantine Basin.

3.3.1 Physical structure

In the 2018 glider mission (Fig. 3), the eddy interior exhibited a hydrographic structure consistent with anticyclonic circulation ~~eddy interior exhibited a coherent hydrographic structure characteristic of an anticyclonic mesoscale eddy~~[R2]. Density surfaces were displaced downward within the eddy, consistent with downwelling-favorable circulation (Fig. 3G), while satellite SST (Fig. 3D–F) and CTD measurements (Fig. 3H) revealed elevated temperatures extending from the surface to approximately 60 m depth relative to the surrounding offshore waters. Together, these observations indicate that the eddy transported a relatively warm coastal-origin water mass into the offshore Levantine Basin. A comparable warm-core signature was also evident in satellite SST during the 2022 event (Fig. 4 D–F). Although CTD measurements were unavailable during this mission because of an instrument malfunction, the satellite observations demonstrated a similar surface thermal structure, indicating that both eddies were associated with the offshore transport of relatively warm coastal waters. This common physical signature provides the framework for comparing their biogeochemical structures, described in the following section.

3.3.2 Biogeochemical structure

Both eddies exhibited a vertical chlorophyll structure that was clearly distinct from adjacent offshore waters (Figs. 3G and 4G). The DCM shoaled from its typical summer depth of approximately 100–120 m in the pelagic Levantine Basin to approximately 50 m, corresponding to the characteristic summer DCM depth over the continental shelf (Fig. A5). Concurrently, chlorophyll concentrations were elevated throughout the upper water column, resulting in a broader vertical chlorophyll distribution than observed in adjacent offshore waters.

The vertical redistribution of chlorophyll was further quantified using chlorophyll anomaly profiles calculated relative to adjacent offshore waters (Methods). Both eddies exhibited a similar anomaly structure, consisting of positive anomalies extending from the surface to approximately 100 m and negative anomalies below the DCM (Figs. 5 and 6). Despite the pronounced

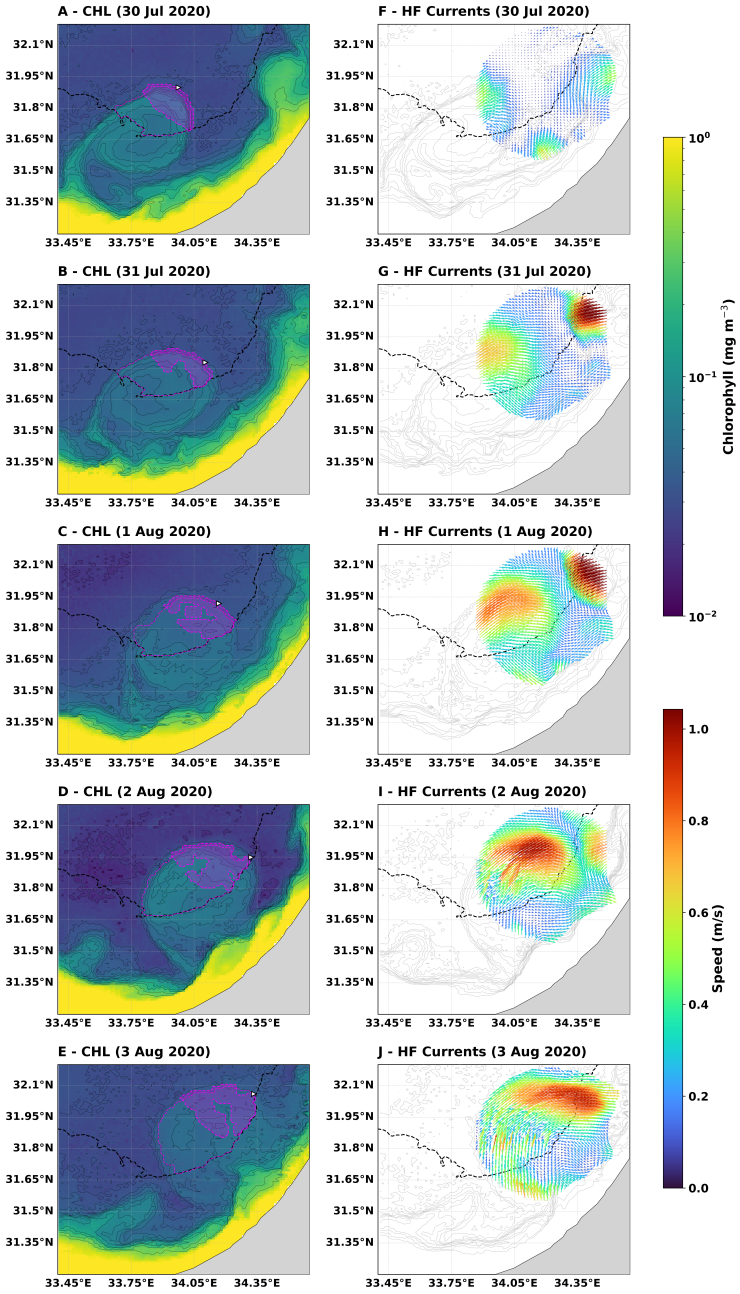

Figure 2. Satellite and HF-radar observations during 30 July–3 August 2020. (A–E) Daily surface chlorophyll maps. The magenta line indicates the identified Chl anomaly and the shaded magenta region marks the frontal boundary used to collocate HF-radar velocity measurements with the chlorophyll-defined mesoscale eddy. The white dot shows the north-easternmost pixel in the eddy area used to calculate eddy propagation velocity across successive days. (F–J) HF-radar surface currents overlaid on CHL contours.

negative anomaly at depth, the vertically integrated chlorophyll anomaly remained positive in both cases. Vertical integration of the anomaly profiles yielded net chlorophyll anomalies of approximately 1.6×10^3 kg~~1,500 kg~~[R1] distributed over an offshore area of about 1,430 km^2 for the 2018 eddy, and approximately 3.5×10^3 kg~~3,500 kg~~[R1] over about 1200 km^2 for the 2022 eddy.

The reproducibility of this vertical chlorophyll structure in two independent glider observations motivated comparison with the offshore *N800* time-series station to determine whether a similar biogeochemical signature was evident in repeated ship-based observations.

3.4 Time-series observations of transported coastal waters

The glider observations revealed a consistent vertical biogeochemical structure associated with coastal mesoscale eddies. To determine whether this transported coastal signature could also be identified independently in repeated offshore observations, we analyzed hydrographic and biogeochemical measurements from the *N800* time-series station during months influenced and not influenced by coastal mesoscale eddies.

Satellite-derived surface chlorophyll imagery indicates that the July and September sampling periods coincided with the passage of coastal mesoscale eddies over the *N800* station (Fig. 7A–B). During these periods, the station exhibited distinct changes in dissolved nutrients, particulate constituents, and the vertical chlorophyll structure relative to the non-eddy summer background.

At *N800*, dissolved silica concentrations in the upper water column increased during the July and September eddy-influenced periods (Fig. 7C). In July, the increase was largely confined to the surface layer, whereas in September, elevated concentrations extended to 50 m depth. Relative to the non-eddy background within the stratified period, upper-layer silica concentrations increased from $0.81 \pm 0.14\ \mu M$ to $1.48\ \mu M$ in July within the upper 20 m ($\Delta Si = 0.67\ \mu M$). In September, upper 50 m concentrations increased from $0.76 \pm 0.14\ \mu M$ to $1.65\ \mu M$ ($\Delta Si = 0.89\ \mu M$). These anomalies exceeded the background variability by factors of approximately 5 and 6, respectively. These changes coincided with enhanced particulate inputs (Fig. 7D). Total inorganic particulate matter, integrated over the upper 180 m from measurements collected at 25, 100, and 180 m, was substantially elevated during July and September relative to the non-eddy background. Mean concentrations increased from $9.3 \pm 2.2\ \mu g\ L^{-1}$ to $31.8\ \mu g\ L^{-1}$ in July and $35.5\ \mu g\ L^{-1}$ in September, corresponding to anomalies of $22.4\ \mu g\ L^{-1}$ and $26.2\ \mu g\ L^{-1}$, respectively. These enhancements exceeded the background variability by factors of approximately 3 and 4, respectively. Particulate Fe concentrations (Fig. 7E) were also elevated during the eddy-influenced periods, with July enrichment extending through the upper 100 m and September enrichment through the upper 180 m. Relative to the non-eddy background within the stratified period, particulate Fe concentrations increased from 22 ± 17 to 102 nM in July within the upper 100 m, and from 28 ± 18 to 92 nM in September within the upper 180 m.~~Relative to the non-eddy background within the stratified period, Fe concentrations increased from 0.022 ± 0.017 to 0.102 in July within the upper 100 m, and from 0.028 ± 0.018 to 0.092 in September within the upper 180 m.~~[R2] These increases exceeded the background variability by factors of approximately 5 and 4, respectively.

The vertical chlorophyll structure also differed from the typical offshore summer profile (Fig. 7F). Profiles from June and August exhibited a pronounced DCM at approximately 120–130 m. In contrast, the July and September profiles showed a

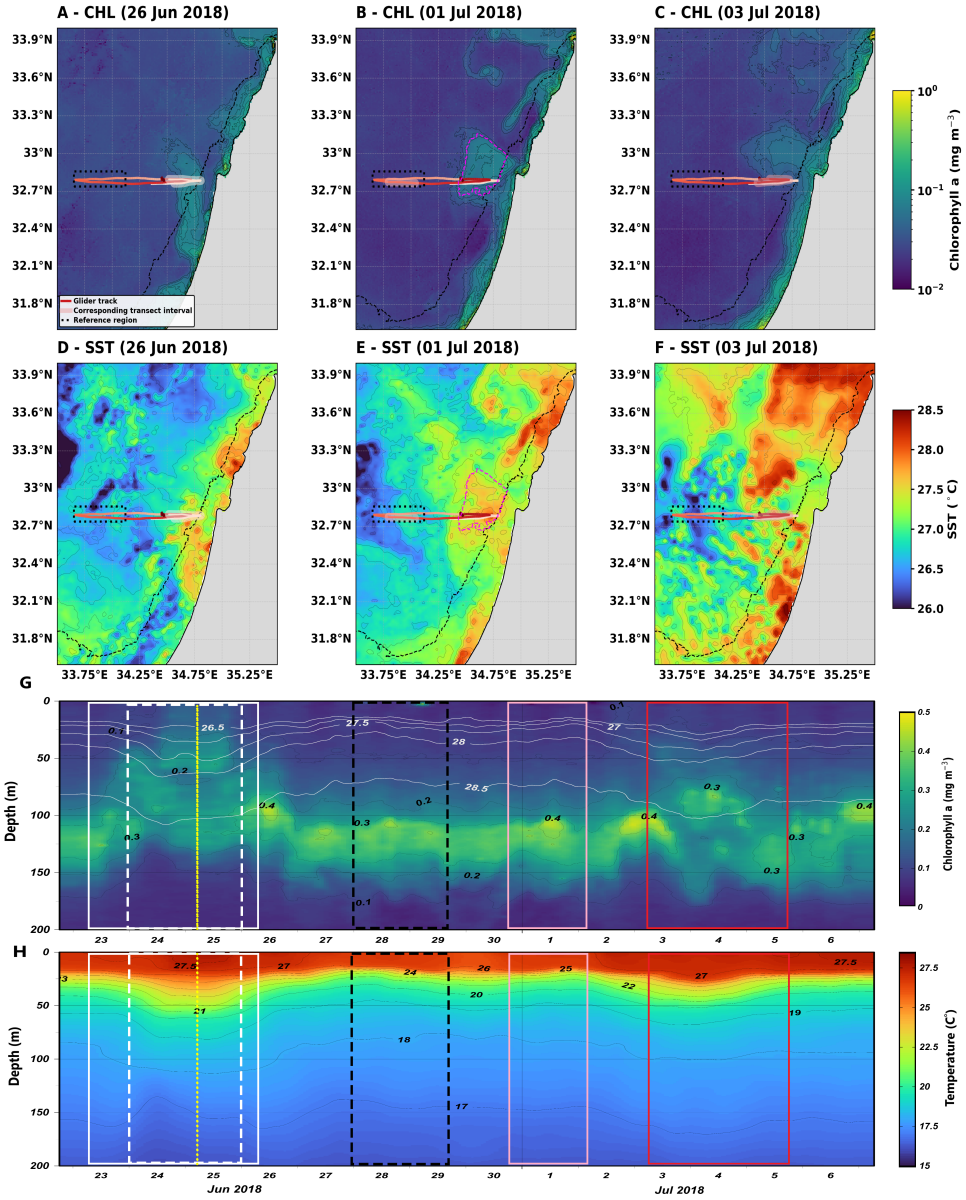

Figure 3. Satellite and glider observations of a coastal eddy during June/July 2018. (A–C) Surface chlorophyll on 26 June, 1 July, and 3 July, with the cumulative glider trajectory colored by time progression. Lightened segments mark the position of the glider at the time of each satellite image. In (B), the magenta contour delineates the identified offshore eddy feature used for the surface-area and chlorophyll-stock calculations. The black dotted rectangle marks the region used for calculation of background conditions. (D–F) Corresponding sea surface temperature (SST) fields for the same dates, shown over the same spatial domain. (G) Glider-derived chlorophyll section (mg m^{-3}), with density anomaly contours (white). Colored rectangles indicate the portions of the transect corresponding to the satellite snapshots, using the same color progression as in (A–C). Dashed white and black rectangles indicate the periods used to calculate the mean eddy and reference profiles, respectively. Dotted yellow lines mark the location of the 700 m isobath.[R2] (H) Glider-derived temperature section (°C), with the same highlighted intervals as in (G).

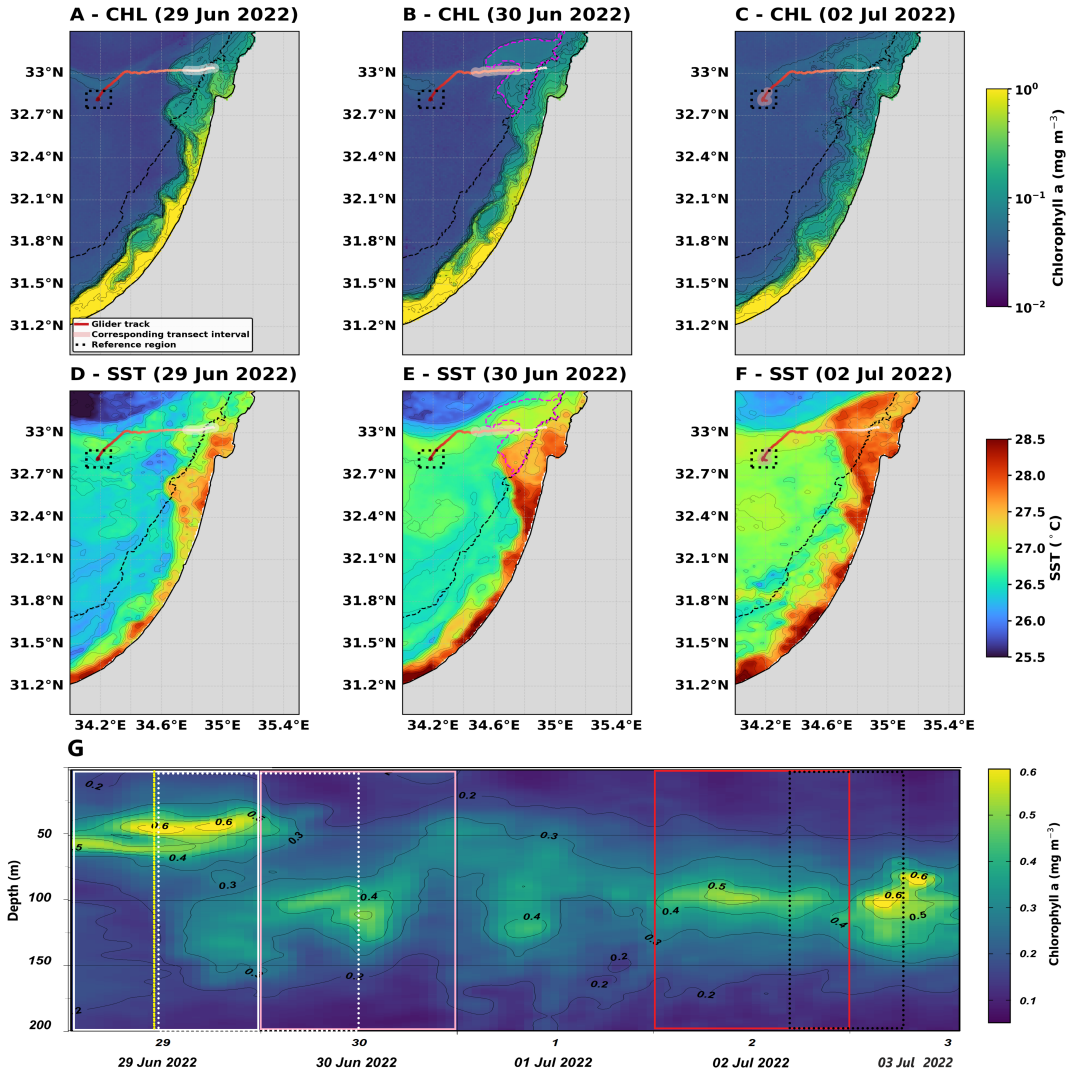

Figure 4. Satellite and glider observations of a coastal eddy during June–July 2022. (A–C) Daily surface chlorophyll with the cumulative glider trajectory overlaid and colored by time progression. Lightened segments mark the position of the glider at the time of each satellite image. In (B), the magenta contour delineates the identified offshore eddy feature used for the surface-area and chlorophyll-stock calculations. The black dotted rectangle marks the region used for calculation of background conditions. (D–F) Corresponding sea surface temperature (SST) fields for the same dates, shown over the same spatial domain. (G) Glider-derived chlorophyll section (mg m^{-3}), with colored rectangles indicating the corresponding portions of the transect, using the same color progression as in (A–C). Dashed white and black rectangles indicate the periods used to calculate the mean eddy and reference profiles, respectively. Dotted yellow lines mark the location of the 700 m isobath.[R2]

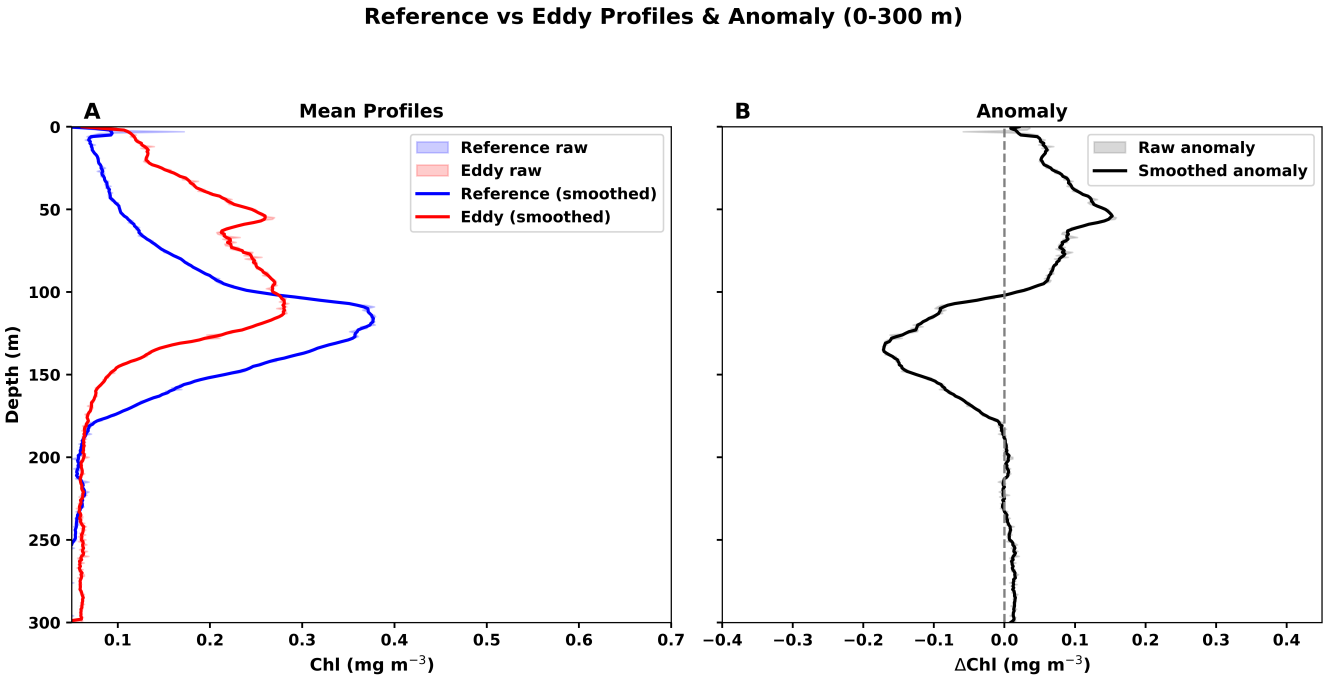

Figure 5. A. Depth profiles of chlorophyll from glider mission M141 during the reference period (28–29 June 2018; blue) and the eddy period (24–25 June 2018; red). (B) Chlorophyll anomaly profile (eddy minus reference; black). Shaded and solid lines denote raw and smoothed profiles, respectively.

broader chlorophyll distribution, with enhanced concentrations extending upward to approximately 50 m in July and 35 m in September. This redistribution resulted in a shoaled and, in some cases, bimodal chlorophyll maximum.~~The vertical chlorophyll structure also differed from the typical offshore summer profile (Fig. 7F). Profiles from June and August exhibited the characteristic offshore Levantine summer pattern, with a pronounced DCM at ~120–130 m. In contrast, the July and September profiles showed a broadened chlorophyll distribution and a reorganization of the vertical structure, including enhanced concentrations higher in the water column. While the increase remained associated with the top of the nutricline, as in background conditions, chlorophyll concentrations were elevated over a thicker depth range extending upward to ~50 m in July and ~35 m in September, resulting in a shoaled and, in some cases, bimodal DCM.~~[R2]

Together, these observations provide independent support for the glider-derived observations of chlorophyll redistribution, with both datasets showing a shoaled and broadened DCM during eddy influence. The *N800* time-series further extends these observations by revealing concurrent increases in dissolved Si and inorganic particulate matter (including particulate Fe, but not total organic matter), providing additional evidence of the biogeochemical signature of transported coastal waters.

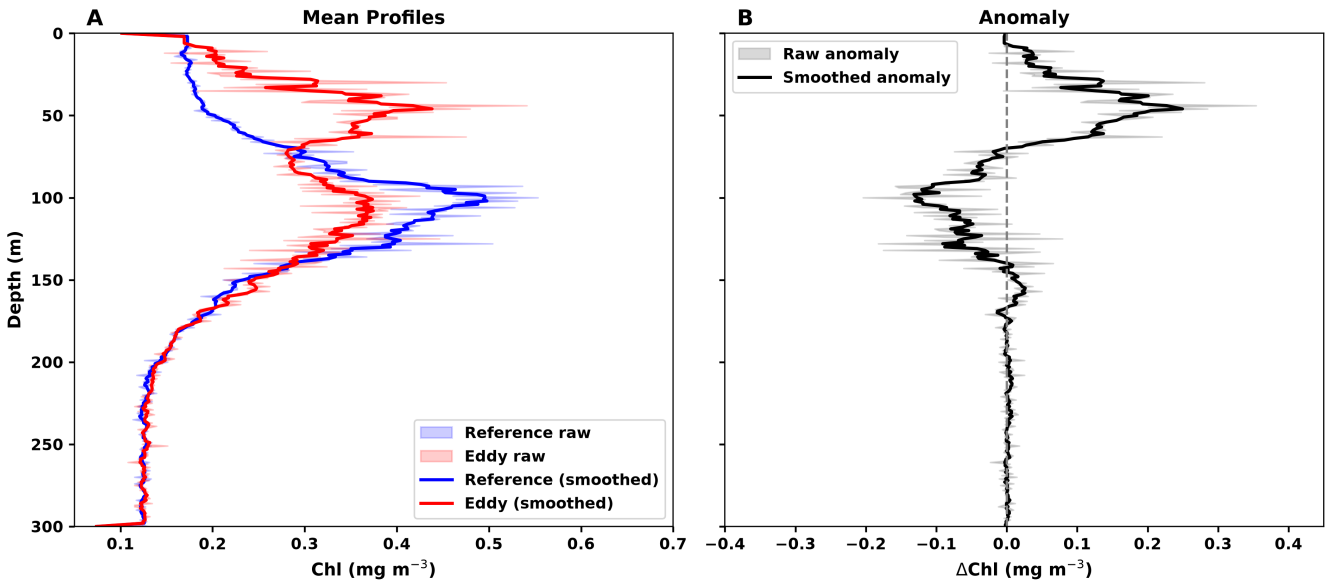

Figure 6. Depth profiles of chlorophyll from glider mission M164 during the reference period (2–3 July 2022; blue) and eddy period (29–30 June 2022; red). (A) Raw and smoothed profiles. (B) Chlorophyll anomaly profile (eddy minus reference).

4 Discussion

4.1 Summertime connectivity and the role of coastal mesoscale eddies

During summer stratification, the Eastern Mediterranean Sea is generally characterized by weak coastal–offshore connectivity. Strong vertical stratification suppresses nutrient resupply to the surface, while the persistent alongshore boundary current limits cross-shore exchange, effectively isolating the offshore Levantine Basin from coastal influences (Estrada, 1996; Rosentraub and Brenner, 2007; Ozer et al., 2022). The Levantine Basin is recognized as a distinct biogeochemical and ecological province within the Mediterranean Sea, characterized by extreme oligotrophy, strong nutrient limitation, and unique hydrodynamic conditions relative to other Mediterranean regions (Ayata et al., 2018). Under these conditions, lateral transport of coastal waters into the open sea is generally expected to be minimal.

The results presented here identify coastal mesoscale eddies as intermittent features that can locally disrupt this summer isolation by transporting chlorophyll and associated biogeochemical signatures from the coastal zone into offshore waters. These eddies form along the coastal boundary current and propagate downstream. Although smaller and faster-propagating than the larger Mediterranean anticyclones described by[R2] Sutyrin et al. (2009) and Poulain et al. (2021), the 2020 HF-radar case (Fig. 2) likewise exhibits rotational velocities substantially exceeding its estimated propagation speed. This relationship is consistent

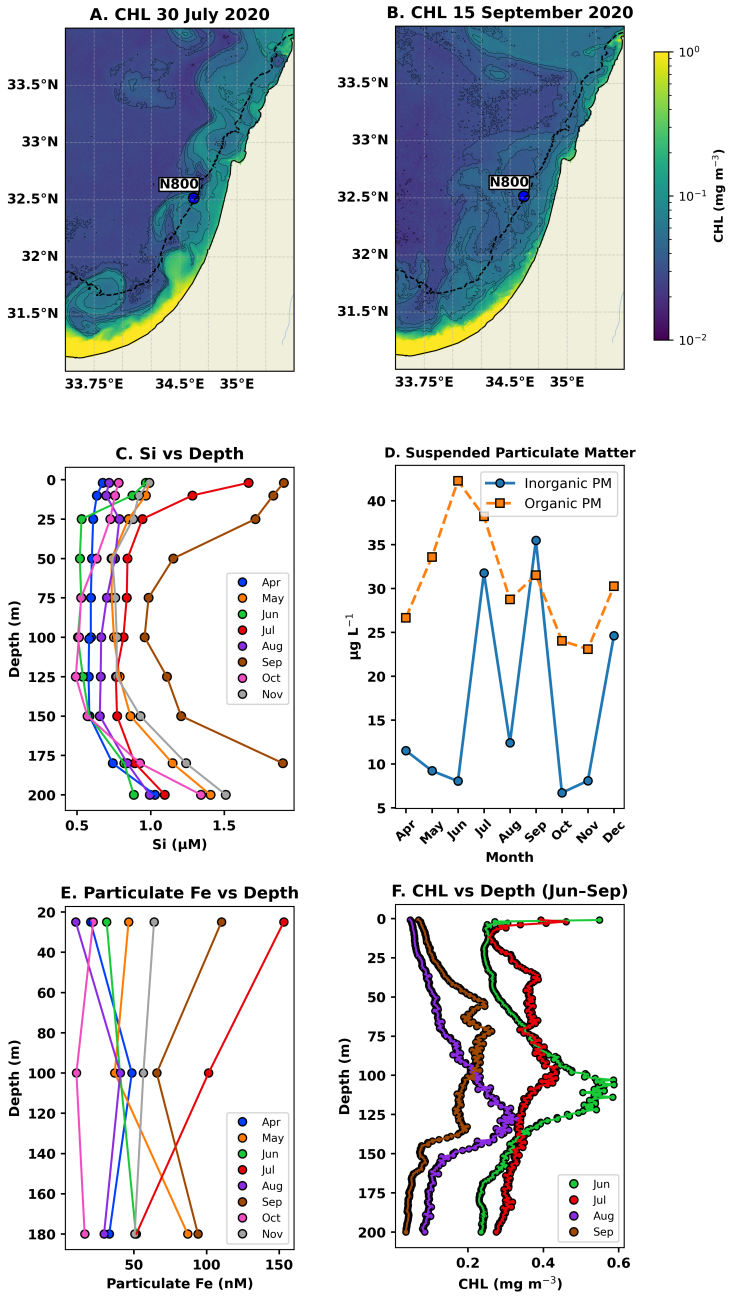

Figure 7. Monthly variability in dissolved and particulate properties at time-series station *N800*. (A–B) Satellite-derived surface chlorophyll fields corresponding to the anomalous sampling dates. (C) Vertical profiles of dissolved silicic acid Si(OH)4 (μM). (D) Monthly integrated suspended particulate matter. (E) Vertical profiles of particulate Fe (nM). (F) Vertical profiles of chlorophyll fluorescence (mg m^{-3}).

with potential fluid trapping[R2] (Chelton et al., 2011), although material retention during propagation was not directly assessed here.[R2] ~~These eddies form along the coastal boundary current and propagate downstream while maintaining a dynamically coherent internal circulation, as evidenced by HF-radar observations showing rotational velocities that substantially exceed their translational speed. While the coastal eddies examined here are smaller and propagate more rapidly than the larger open-ocean anticyclones described elsewhere in the Mediterranean, both exhibit the characteristic kinematics of coherent vortices, with internal rotational velocities greatly exceeding translational speeds, allowing water masses to remain trapped within the eddy core during propagation~~[R2] While biological tracers may exhibit small spatial offsets relative to the underlying dynamical structures, chlorophyll distributions have been shown to provide reliable indicators of mesoscale circulation features when combined with HF-radar observations (Fanelli et al., 2024; Navarro and Ruiz, 2006). The close agreement observed here between the chlorophyll-defined frontal boundary and the regions of strongest azimuthal velocity suggests that any such offset was small relative to the scale of the eddy and does not affect the interpretation of its kinematics. Coastal mesoscale features along the Levantine margin have been documented through drifter observations of anticyclonic eddy detachment and offshore propagation[R1] (Gertman et al., 2010), regional analyses of surface circulation[R1] (Menna et al., 2012), and satellite observations of coastal-water pinching-off events and seasonal frontal variability[R1] (Baaklini et al., 2024; Akpınar, 2024). Numerical studies further describe the three-dimensional circulation and boundary-current instabilities associated with these features[R1] (Estournel et al., 2021; Verma et al., 2024). Efrati et al. (2013) extended this characterization through hydrographic and biogeochemical sampling of a coastal intrusion, identifying a distinct water-mass signature within the upper approximately 25 m and estimating its offshore volume flux. These findings provide a foundation for examining the vertical biogeochemical structure associated with coastal eddy transport below the surface mixed layer.[R1] ~~Similar mesoscale features have been documented along the Levantine coast in observations and models, and satellite data indicate that they recur during summer.~~[R1] Their episodic nature suggests that a portion of coastal–offshore exchange during the stratified season occurs through discrete transport events rather than persistent background exchange. Importantly, the significance of these events does not lie in their contribution to the annual cross-shore transport budget, nor in replacing the much stronger basin-scale connectivity that characterizes winter. Rather, their importance lies in temporarily overcoming the strong coastal–offshore separation that normally persists during summer. In this sense, the primary comparison addressed in this study is between offshore waters influenced by coastal mesoscale eddies and the surrounding offshore environment under typical summer conditions, rather than between summer and winter transport regimes. By transporting a distinct~~coherent~~[R2] coastal water-mass signature into the oligotrophic offshore basin, these eddies create transient connections between two regions that are otherwise largely isolated during the stratified season.

4.2 Vertical structure and coastal water-mass signatures

The influence of coastal mesoscale eddies extends beyond surface tracer redistribution and involves a consistent reorganization of the upper water column. Glider observations demonstrate that eddy interiors are characterized by elevated chlorophyll concentrations and a pronounced shoaling and broadening of the DCM relative to background offshore conditions. Such a shallow DCM contrasts with the deep, well-defined offshore DCM typically observed during summer stratification in the Levantine Basin (Mignot et al., 2014; Teruzzi et al., 2021; Ediger and Yilmaz, 1996; Ben-Ezra et al., 2024).

The vertical structure of these features provides insight into their underlying dynamics and origin. In the primary glider case (Fig. 3), the broadened and shoaled DCM occurs in conjunction with downward-displaced density surfaces, consistent with anticyclonic, downwelling-favorable circulation. This combination supports lateral advection of a preconditioned coastal water mass as the explanation for enhanced upper-layer chlorophyll, rather than local upwelling within the eddy (Moore et al., 2007). HF-radar observations independently show anticyclonic surface circulation during the 2020 event (Fig. 2). Together, the glider and HF-radar observations support anticyclonic circulation in these two cases, although circulation polarity could not be established for every sampled event. Regional simulations show that, during summer, the boundary current flows closer to the coastline and develops narrow bands of concentrated anticyclonic vorticity. These bands become unstable and roll up into anticyclonic spirals, while smaller cyclonic spirals occasionally develop at their peripheries through secondary instabilities[R1] (Verma et al., 2024). Such cyclonic features may also contribute to coastal-water redistribution, but their biogeochemical effects are not resolved by the observations presented here.[R1] Elevated surface and subsurface temperatures observed within the eddy are consistent with this interpretation. Independent ship-based observations at the time-series station *N800* provide additional evidence supporting these findings. Periods influenced by coastal mesoscale eddies were characterized by elevated silicate concentrations in the upper water column, increased amounts of fine-grained inorganic particles, and a modified vertical chlorophyll structure. Consistent with this interpretation, CTD observations at station *N800* show lower surface salinity and higher surface temperature during the July eddy (Fig. A4A,B), indicative of coastal-origin water previously described for the southeastern Levantine Basin (Ozer et al., 2022). Rather than exhibiting the typical, well-defined DCM, chlorophyll began increasing at the top of the nutricline, as under normal conditions, but the distribution was broadened and intensified upward, extending to depths of approximately 35–50 m. Independent cross-shelf cruise observations show that the chlorophyll maximum is typically bottom-associated at approximately 50–60 m (the average depth of the shelf in this region) over the continental shelf, before deepening beyond the shelf break to form the well-defined offshore DCM at approximately 100–130 m (Fig. A5), supporting the interpretation that the shallower chlorophyll structure observed within the eddy retains a coastal shelf signature. Advection of preconditioned coastal water, therefore, provides a plausible explanation for the N800 anomalies without requiring additional modification during transport. Sediment resuspension during eddy formation could nevertheless increase the particle load available for offshore export, a pathway documented for anticyclonic eddies[R2] (Washburn et al., 1993; Crusius et al., 2017). This would be expected to enhance particulate Fe and turbidity within the transported layer, without necessarily producing a corresponding chlorophyll maximum. Resuspension could also entrain sediment-associated photosynthetic microorganisms [R2](Rubin-Blum et al., 2022), while nutrient release could potentially support subsequent growth. These processes may contribute to the observed signal, although the measurements presented here are insufficient to distinguish their contributions from the transport of material already present in coastal waters.[R2] ~~A plausible mechanism is that, as the coastal eddy forms, its current is sufficiently strong to resuspend the uppermost sediments of the adjacent shelf, which includes fine-grained sediment. This resuspended layer contains benthic phytoplankton and is likely enriched in nutrients due to in situ heterotrophic bacterial activity. Consequently, the eddy core is transported from the shelf into pelagic waters, carrying elevated dissolved and particulate nutrient concentrations (Fig. 7). The dissolved nutrients introduced to pelagic waters have the capacity to stimulate new primary production which, combined with sinking particles with benthic phytoplankton attached,~~

~~contribute to the observed enhanced chlorophyll signal.~~[R2] Vertical chlorophyll structure at station *N800* closely resembled that observed during the glider missions. Although anomaly profiles were not explicitly calculated for the *N800* data, the vertical distributions during eddy-influenced months showed enhanced chlorophyll in the upper 100 m and comparatively reduced concentrations at greater depths, consistent with the two-layer anomaly structure identified from the glider analysis. PAR profiles from the *N800* cruises (Fig. A4C) further showed a divergence beginning near 40 m, with lower subsurface PAR during the July and September eddy periods relative to the June and August reference profiles. This reduction in light penetration provides a plausible mechanism for the observed deep chlorophyll suppression. The elevated chlorophyll concentrations and increased suspended particulate matter associated with eddy influence likely enhanced light attenuation in the upper water column, further reducing subsurface PAR and contributing to the negative anomaly at depth, consistent with established relationships between particle concentrations, optical attenuation, and underwater light availability (Babin et al., 2003; Neukermans et al., 2014; Morel and Maritorena, 2001). Coastal waters in the Eastern Mediterranean receive terrestrial and benthic nutrient inputs; however, anti-estuarine circulation and rapid biological uptake limit the accumulation of nutrients and prevent the development of a persistent cross-shore nutrient gradient (Kress and Herut, 1998; Ben-Ezra et al., 2023; Krom et al., 2010). Consequently, coastal biogeochemical signals are often short-lived or spatially heterogeneous, and may only become clearly expressed offshore when transported within mesoscale features (Efrati et al., 2013). The recurrence of these vertical signatures across various sampling strategies suggests that the observed reorganization reflects a persistent property of the advected water mass rather than transient biological responses to local forcing.

4.3 Event-scale offshore redistribution under stratified conditions

The vertical reorganization associated with coastal mesoscale eddies results in a measurable redistribution of chlorophyll within the offshore water column. By combining vertically integrated chlorophyll anomaly profiles with the offshore surface area of individual eddies, the results provide event-scale estimates of the excess chlorophyll transported offshore during summer stratification (1.6×10^3-3.5×10^3 kg~~1,500-3,500 kg~~[R1] per eddy). Similar event-based approaches have been used to assess eddy-driven transport in other oligotrophic systems (Gerin et al., 2009; Martin, 2003). For both glider-sampled eddies, the vertically integrated chlorophyll anomaly was positive, reflecting the combined effects of elevated surface concentrations and a shoaled DCM relative to background offshore conditions. Although the absolute magnitudes differed between events, the consistent sign of the anomaly indicates that coastal mesoscale eddies can act as net exporters of chlorophyll and nutrients into the offshore Levantine Basin during summer.

In an ultra-oligotrophic system such as the eastern Levantine Basin (Krom et al., 2005; Herut et al., 2000), even modest event-scale anomalies may be biogeochemically relevant. Background offshore chlorophyll concentrations are extremely low, and phytoplankton biomass during summer is largely confined to a narrow depth range near the nutricline (Mignot et al., 2014; Teruzzi et al., 2021). More generally, oligotrophic ecosystems are particularly sensitive to physical transport processes because biological production is strongly constrained by the availability and redistribution of nutrients and biomass, allowing mesoscale and submesoscale circulation features to exert a disproportionate influence on ecosystem structure and productivity (Levy et al., 2001). Because eddy occurrence is episodic and interception by in situ platforms is limited, these estimates cannot

be robustly extrapolated to seasonal or basin-wide budgets and should be interpreted as first-order, event-scale indicators of offshore redistribution.

4.4 Broader context and limitations

Coastal eddies have been shown to facilitate cross-shelf exchange in a range of boundary current systems, often transporting nutrient-rich waters offshore and enhancing biological productivity (Flos and Tintoré, 1990; Espinosa-Carreón et al., 2012; Wang et al., 2018). In many of these regions, however, coastal–offshore contrasts in nutrients and biomass are substantially larger than in the Eastern Mediterranean, and background productivity is higher.

The Levantine Basin represents a limiting case, where nutrient concentrations and surface chlorophyll are among the lowest observed globally (Krom et al., 2005; Pujo-Pay et al., 2011). In this context, the presence of detectable biogeochemical signatures associated with coastal eddies highlights that even modest coastal enrichment can be preserved and transported offshore when associated with propagating coastal mesoscale structures~~when embedded within dynamically coherent mesoscale structures~~[R2]. The Eastern Mediterranean therefore provides a useful natural laboratory for examining eddy-driven exchange under ultra-oligotrophic conditions. Beyond the redistribution of chlorophyll and nutrients, mesoscale and sub-mesoscale transport processes may also influence the composition and organization of offshore plankton communities. Efrati et al. (2013) suggested that transport barriers surrounding such intrusions could maintain localized niches supporting distinct plankton communities. Consistent with this possibility,[R1] Moore et al. (2007) identified modified shelf phytoplankton communities within anticyclonic eddies transported offshore from Western Australia. The coastal water-mass signatures observed here provide physical and biogeochemical context for these potential ecological effects, although plankton-community composition was not measured in this study.[R1] In oligotrophic environments, where biological responses are often strongly resource-limited, episodic coastal inputs transported by mesoscale features may affect ecosystem structure in addition to biomass distribution (Lévy et al., 2018; Chenillat et al., 2024). ~~More broadly, fronts, filaments, and mesoscale circulation features are increasingly recognized as important organizers of biological heterogeneity in oligotrophic oceans, influencing the spatial distribution of plankton communities and the transfer of energy across multiple trophic levels.~~[R1]

The coastal location and relatively small size of these features present challenges for conventional SSH-based analyses. Gridded altimetry products in the Mediterranean typically have resolutions comparable to the regional Rossby radius and may only partially resolve mesoscale structures forming close to the coastline, where land contamination and interpolation further increase uncertainty. Consequently, the chlorophyll signal provides a more direct tracer of coastal-origin transport for the events investigated here. In addition to their small spatial scale and coastal location, the relatively rapid evolution of these coastal eddies likely further limits their detectability in gridded SSH products. Unlike the larger offshore mesoscale eddies that can often be tracked continuously over weeks to months, the surface expression of the coastal eddies investigated here evolves on much shorter timescales. Successive chlorophyll observations, and SST where thermal contrast is sufficient, indicate that individual events typically persist for several days to approximately one week before undergoing substantial changes in position, morphology, or intensity. As a result, ocean color and SST provide the most effective means of identifying and tracking these transient coastal features, whereas their SSH signature is often weak or unresolved. The present results complement previous

SSH-based descriptions of Levantine mesoscale circulation and long-lived anticyclones (Barboni et al., 2021) by resolving the biogeochemical imprint of smaller coastal transport features. Likewise, whereas BOUM observations emphasized the properties of large anticyclonic eddy interiors (Moutin et al., 2012), the present work focuses on coastal-origin water masses exported offshore and their vertical biogeochemical signatures.

The conclusions drawn here are subject to several observational limitations. Interception of coastal mesoscale eddies by autonomous gliders and ship-based sampling is inherently opportunistic and constrained by platform trajectories and sampling schedules. In addition, the export estimates rely on assumptions regarding eddy geometry, representativeness of vertical profiles, and the choice of background reference conditions. While these assumptions are physically motivated and internally consistent, they introduce uncertainty that limits quantitative extrapolation beyond the sampled events. Although the present work focuses on individual events, the recurrent occurrence of coastal mesoscale activity suggests that their cumulative contribution to offshore exchange warrants future statistical investigation.

5 Conclusions

Coastal mesoscale eddies provide an intermittent but effective pathway for cross-shore exchange during summer stratification in the Eastern Mediterranean, exporting coastal water into the otherwise isolated offshore Levantine Basin. Although these features are predominantly anticyclonic and typically associated with downwelling and low productivity in pelagic regions, their formation in proximity to the coast allows them to entrain relatively enriched waters. As a result, they transport elevated chlorophyll, nutrients, and suspended particulate matter offshore, along with a distinct vertical structure characterized by a shallow, often bimodal DCM. The analysed coastal mesoscale eddies extended over offshore areas of approximately 1200–1430 km^2 and were associated with positive vertically integrated chlorophyll anomalies corresponding to estimated offshore redistribution of approximately 1.6×10^3-3.5×10^3 kg~~1,500-3,500 kg~~[R1] of chlorophyll per eddy. The transported water masses exhibited a shoaling of the DCM from typical offshore depths of approximately 120–130 m to 50 m within the eddy interior and were accompanied by elevated nutrient and particulate signatures. These findings highlight how mesoscale dynamics can modify the expected biogeochemical role of anticyclonic eddies and emphasize their importance as episodic drivers of offshore redistribution in ultra-oligotrophic environments.

Data availability. This study has been conducted using E.U. Copernicus Marine Service;
DOI: 10.48670/moi-00300 (product name: $OCEANCOLOUR_MED_BGC_L4_MY$).
DOI: 10.48670/moi-00299 (product name: $OCEANCOLOUR_MED_BGC_L3_MY$_009_143).
DOI: 10.48670/moi-00141 (product name: $SEALEVEL_EUR_PHY_L4_MY$_008_068).
DOI: 10.48670/moi-00172 (product name: $SST_MED_SST_L4_NRT_OBSERVATIONS$_010_004_$c_V2$).
HF Radar data is available at: https://app.hubocean.earth/catalog/dataset/f0b38644-7cb3-4fdc-bec7-081c52b591fa/hf-radar?
Glider data from mission M141 is available at:
https://app.hubocean.earth/catalog/dataset/52369e62-41c0-487f-91d1-9b8c01a8b618/glider-mission-m141?

Glider data from mission M164 is available at:

https://app.hubocean.earth/catalog/dataset/267dc865-1d7f-4f3d-8560-ce456b3903c4/glider-mission-m164?

Cruise data from the *N800* station is available at: https://haifauniversity.shinyapps.io/Public_Download_app_06_2022/

Cruise data from the *Haifa Section* cruises is available at:

https://app.hubocean.earth/catalog/dataset/7a463a3e-972b-4034-a348-309440e64408/haifa-section-cruises-chlorophyll-2018-2021?

Appendix A

Table A1. Sensitivity of offshore eddy surface-area estimates to the use of L3 and L4 satellite chlorophyll products. The same detection procedure described in Section 2.2.1 was applied independently to L3 and gap-filled L4 chlorophyll fields for the dates shown in Fig. A1. Absolute and relative differences were calculated as L4 minus L3, with the relative difference expressed as a percentage of the L3 estimate. The comparison shows negligible sensitivity of the detected offshore surface area to product level for both events.

Eddy event	Date	L3 area (km^2)	L4 area (km^2)	Difference (km^2)	Difference (%)
2018 glider event	1 July 2018	1431.6	1433.0	+1.4	+0.09
2022 glider event	30 June 2022	1202.8	1202.8	0.0	0.00

Table A2. Comparison of eddy propagation velocities and detected offshore feature areas derived from L3 and L4 satellite chlorophyll products. The detection procedure described in Section 2.2.2 was applied independently to L3 and gap-filled L4 chlorophyll fields for the dates shown in Fig. A2. Propagation velocities were calculated from frontal-boundary displacements between consecutive images; signed differences are L4 minus L3. Feature areas represent the detected chlorophyll anomaly seaward of the 700 m isobath, rather than total eddy area. Both products show a progressive increase in offshore feature area and closely comparable propagation velocities.

Propagation velocity comparison			
Period	**L3 velocity (km day^{-1})**	**L4 velocity (km day^{-1})**	**Difference (km day^{-1})**
30 Jul – 31 Jul 2020	14.47	14.47	0.00
31 Jul – 1 Aug 2020	11.81	11.81	0.00
1 Aug – 2 Aug 2020	14.94	14.94	0.00
2 Aug – 3 Aug 2020	13.57	12.45	−1.12
Daily offshore feature area comparison			
Date	**L3 area (km^2)**	**L4 area (km^2)**	
30 Jul 2020	607	607	
31 Jul 2020	667	667	
1 Aug 2020	890	895	
2 Aug 2020	1185	1167	
3 Aug 2020	1368	1364	

Table A3. Analytical precision and limits of detection (LOD) for dissolved nutrient measurements used in the *N800* analysis.

Determinant	Usual range (nM)	Precision	LOD (nM)	Detector
DIP	0–125	2	6	LWCC
Nitrate	0–1000	63	13	1 cm cell spectrophotometer
Ammonium	0–500	6	5	JASCO fluorometer
Silicate	0–2000	7	11	1 cm cell spectrophotometer
TDP	0–200	5	2	LWCC

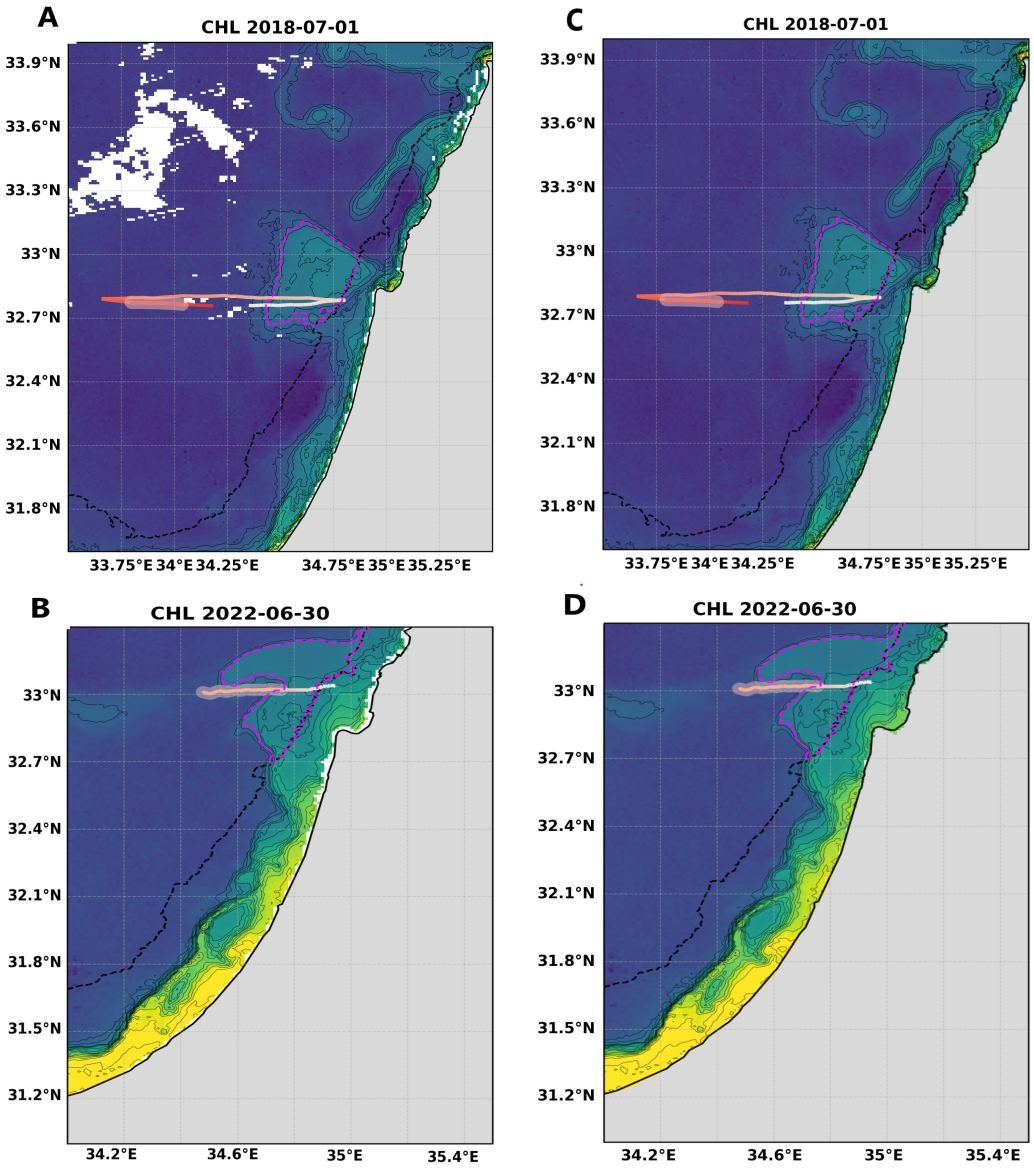

Figure A1. Comparison of L3 and L4 satellite chlorophyll products for the two coastal mesoscale eddies identified using the detection method described in Section 2.2.1 and presented in Fig. 3B and Fig. 4B. (A, B) L3 chlorophyll fields for 1 July 2018 and 30 June 2022, respectively. (C, D) Corresponding L4 chlorophyll fields for the same dates. Magenta contours indicate the offshore eddy boundaries identified using the procedure described in Section 2.2.1. The black dashed line denotes the 700 m isobath, and the glider trajectories are overlaid for reference. The comparison shows that the same offshore transport features are identified in both products, while the gap-filled L4 fields provide a more spatially continuous representation of the chlorophyll distribution.

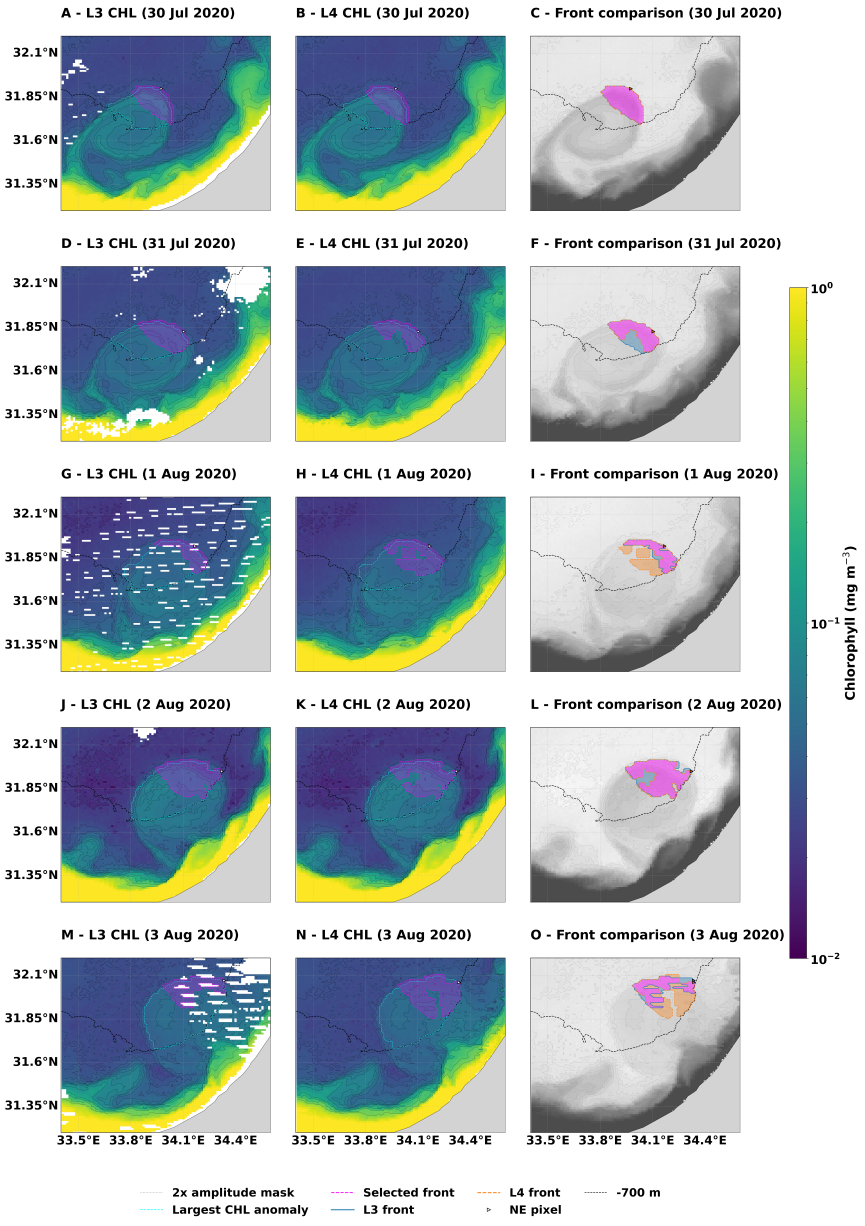

Figure A2. Comparison of L3 and L4 satellite chlorophyll products for the coastal mesoscale eddy analyzed using the frontal-boundary detection method described in Section 2.2.2 and the HF-radar analysis presented in Fig. 2. (A/D/G/J/M) L3 chlorophyll fields from 30 July to 3 August 2020. (B/E/H/K/N) Corresponding L4 chlorophyll fields for the same dates. Magenta contours indicate the eddy frontal boundaries identified using the gradient-based detection procedure described in Section 2.2.2. The black dashed line denotes the 700 m isobath. Panels C, F, I, L, and O compare the frontal regions identified independently from the L3 and L4 products. The comparison demonstrates that the same coastal mesoscale eddy~~the same dynamically coherent coastal mesoscale eddy~~[R2] and its frontal boundary are identified using both products, while the gap-filled L4 fields provide a more spatially continuous representation of the chlorophyll distribution.

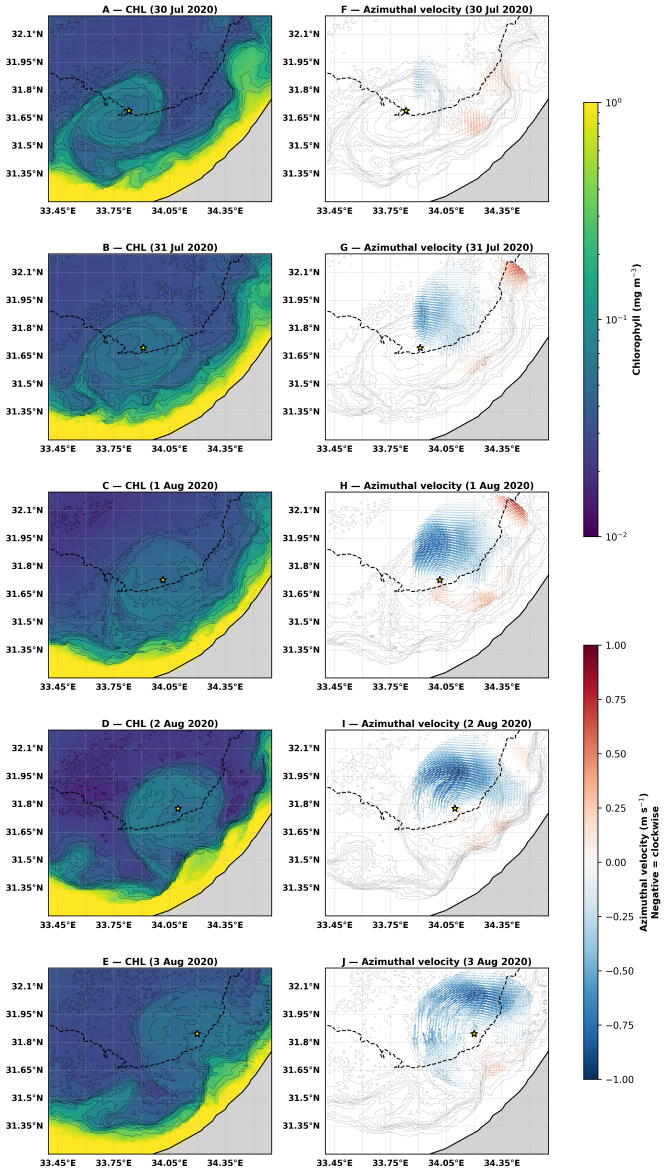

Figure A3. Satellite chlorophyll and azimuthal surface velocities during 30 July–3 August 2020. (A–E) Daily Level-4 chlorophyll concentrations. (F–J) Azimuthal components of the approximately three-hour-averaged HF-radar velocities, calculated relative to the manually selected daily eddy centres (yellow stars). Arrow direction and length represent the tangential velocity component; colours indicate its signed magnitude, with negative values (blue) denoting clockwise (anticyclonic) rotation and positive values (red) counterclockwise (cyclonic) rotation. Grey contours in F–J show the corresponding chlorophyll fields. Black dashed lines mark the 700 m isobath.

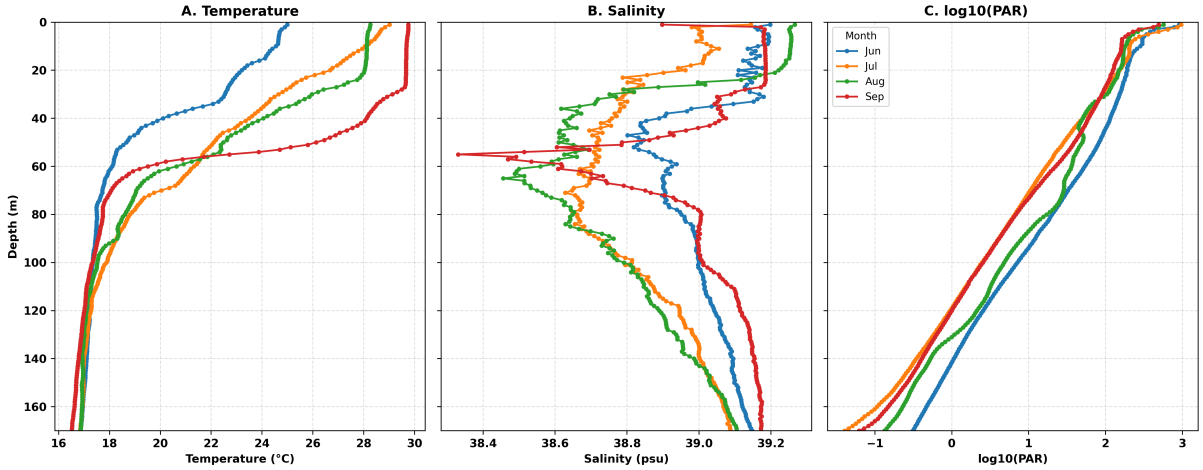

Figure A4. Vertical profiles of A. **temperature**, B. **salinity**, and C. $\log_{10}(\mathrm{PAR})$ at station *N800* during June–September 2020. Profiles are derived from individual ship-based measurements and shown from the surface to 170 m depth. Photosynthetically active radiation (PAR) was recalculated from measured values using a 3 m depth-smoothed moving average prior to log-transformation.

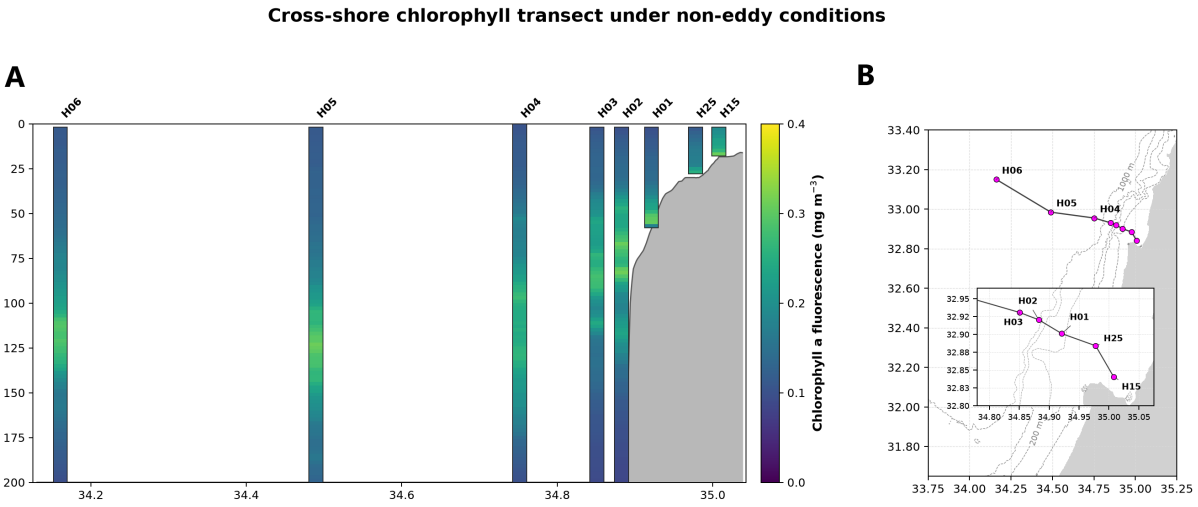

Figure A5. A. Mean summer (August–September) chlorophyll transect across the continental shelf based on the Haifa Section cruises (2018–2021). The section represents the average of repeated summertime CTD measurements of the eight sampling stations shown in panel (B), extending from the nearshore shelf to the open Levantine Basin. The transect illustrates the characteristic transition from the bottom-associated coastal chlorophyll maximum over the continental shelf to the DCM in offshore waters.

Author contributions. Y.F. compiled, processed, and analyzed the satellite and glider data. T.O. collected and processed the glider data. T.BE., M.D.K., A.T., and M.T. collected, processed, analysed, and interpreted the cruise data. Y.T. collected and processed the HF radar data. Y.L. and E.B. oversaw the research. Y.F., Y.L, M.D.K., T.O., T.BE. and E.B. interpreted the results. Y.F. led the writing of the paper with contributions from all coauthors.

Competing interests. The authors declare they have no competing interests.

Acknowledgements. This research has been supported by the Israel Science Foundation (grant no. 1266/23) and by funding from the Planning and Budgeting Committee (PBC) Israel Program for Marine Research Centers (2024-2028) for the Project “Bridging the variability gaps to resolve the long-term impacts of climate change on the SE Levantine basin: development and networking of advanced marine research infrastructures". The glider mission M141 was financed by the Italian Ministry of Foreign Affairs and the Israeli Ministry of Innovation, Science and Technology (as part of the MELMAS project). The cruise data in this study were made possible by the MKMRS monitoring cruise series, as well as the Charney School of Marine Sciences, with support from the captain and crew of the MedExplorer and EcoOcean. The authors acknowledge the use of ChatGPT (OpenAI) for assistance with language editing and phrasing of parts of the manuscript. All scientific content, interpretations, and conclusions are solely those of the authors.

References

Akpınar, A.: Seasonal and Interannual Variability in Sea Surface Temperature Fronts in the Levantine Basin, Mediterranean Sea, Journal of Marine Science and Engineering, 12, https://doi.org/10.3390/jmse12081249, 2024.

Alkalay, R., Zlatkin, O., Katz, T., Herut, B., Halicz, L., Berman-Frank, I., and Weinstein, Y.: Carbon export and drivers in the southeastern Levantine Basin, Deep Sea Research Part II: Topical Studies in Oceanography, 171, 104 713, https://doi.org/10.1016/j.dsr2.2019.104713, revisiting the Eastern Mediterranean: Recent knowledge on the physical, biogeochemical and ecosystemic states and trends (Volume II), 2020.

Amitai, Y., Lehahn, Y., Lazar, A., and Heifetz, E.: Surface circulation of the eastern Mediterranean Levantine basin: Insights from analyzing 14 years of satellite altimetry data, Journal of Geophysical Research: Oceans, 115, https://doi.org/10.1029/2010jc006147, 2010.

Ayata, S.-D., Irisson, J.-O., Aubert, A., Berline, L., Dutay, J.-C., Mayot, N., Nieblas, A.-E., D'Ortenzio, F., Palmiéri, J., Reygondeau, G., Rossi, V., and Guieu, C.: Regionalisation of the Mediterranean basin, a MERMEX synthesis, Progress in Oceanography, 163, 7–20, https://doi.org/10.1016/j.pocean.2017.09.016, special issue of MERMEX project: Recent advances in the oceanography of the Mediterranean Sea, 2018.

Azov, Y.: Seasonal patterns of phytoplankton productivity and abundance in nearshore oligotrophic waters of the Levant Basin (Mediterranean), Journal of Plankton Research, 8, 41–53, https://doi.org/10.1093/plankt/8.1.41, 1986.

Baaklini, G., Brajard, J., Issa, L., Fifani, G., Mortier, L., and El Hourany, R.: Monitoring the coastal–offshore water interactions in the Levantine Sea using ocean color and deep supervised learning, Ocean Science, 20, 1707–1720, https://doi.org/10.5194/os-20-1707-2024, 2024.

Babin, M., Stramski, D., Ferrari, G. M., Claustre, H., Bricaud, A., Obolensky, G., and Hoepffner, N.: Variations in the light absorption coefficients of phytoplankton, nonalgal particles, and dissolved organic matter in coastal waters around Europe, Journal of Geophysical Research: Oceans, 108, https://doi.org/10.1029/2001JC000882, 2003.

Barale, V., Jaquet, J.-M., and Ndiaye, M.: Algal blooming patterns and anomalies in the Mediterranean Sea as derived from the SeaWiFS data set (1998–2003), Remote Sensing of Environment, 112, 3300–3313, https://doi.org/10.1016/j.rse.2007.10.014, earth Observations for Marine and Coastal Biodiversity and Ecosystems Special Issue, 2008.

Barboni, A., Lazar, A., Stegner, A., and Moschos, E.: Lagrangian eddy tracking reveals the Eratosthenes anticyclonic attractor in the eastern Levantine Basin, Ocean Science, 17, 1231–1250, https://doi.org/10.5194/os-17-1231-2021, 2021.

Barrick, D. E.: Extraction of wave parameters from measured HF radar sea-echo Doppler spectra, Radio Science, 12, 415–424, https://doi.org/10.1029/RS012i003p00415, 1977.

Belkin, N., Guy-Haim, T., Rubin-Blum, M., Lazar, A., Sisma-Ventura, G., Kiko, R., Morov, A. R., Ozer, T., Gertman, I., Herut, B., and Rahav, E.: Influence of cyclonic and anticyclonic eddies on plankton in the southeastern Mediterranean Sea during late summertime, Ocean Science, 18, 693–715, https://doi.org/10.5194/os-18-693-2022, 2022.

Ben-Ezra, T., Reich, T., Tsemel, A., Berman-Frank, I., Lehahn, Y., Sher, D., Suari, Y., and Krom, M.: Nutrient dynamics across the Israeli coastal shelf: An unusual oligotrophic coastal system, Continental Shelf Research, 266, 105 103, https://doi.org/10.1016/j.csr.2023.105103, 2023.

Ben-Ezra, T., Blachinsky, A., Gozali, S., Tsemel, A., Fadida, Y., Tchernov, D., Lehahn, Y., Tsagaraki, T. M., Berman-Frank, I., and Krom, M.: Interannual changes in nutrient and phytoplankton dynamics in the Eastern Mediterranean Sea (EMS) predict the consequences of climate change; results from the Sdot-Yam Time-series station 2018-2022, bioRxiv, https://doi.org/10.1101/2024.06.24.600321, 2024.

Berman, T., Townsend, D., Elsayed, S., Trees, C., and Azov, Y.: Optical transparency, chlorophyll and primary productivity in the eastern mediterranean near the israeli coast, Oceanologica Acta, 7, 367–372, https://archimer.ifremer.fr/doc/00131/24219/, 1984.

Berthon, J.-F. and Zibordi, G.: Bio-optical relationships for the northern Adriatic Sea, International Journal of Remote Sensing - INT J REMOTE SENS, 25, 1527–1532, https://doi.org/10.1080/01431160310001592544, 2004.

Birol, F., Bignalet-Cazalet, F., Cancet, M., Daguze, J.-A., Fkaier, W., Fouchet, E., Léger, F., Maraldi, C., Niño, F., Pujol, M.-I., and Tran, N.: Understanding uncertainties in the satellite altimeter measurement of coastal sea level: insights from a round-robin analysis, Ocean Science, 21, 133–150, https://doi.org/10.5194/os-21-133-2025, 2025.

Chelton, D. B., deSzoeke, R. A., Schlax, M. G., Naggar, K. E., and Siwertz, N.: Geographical Variability of the First Baroclinic Rossby Radius of Deformation, Journal of Physical Oceanography, 28, 433 – 460, https://doi.org/10.1175/1520-0485(1998)028<0433:GVOTFB>2.0.CO;2, 1998.

Chelton, D. B., Schlax, M. G., and Samelson, R. M.: Global observations of nonlinear mesoscale eddies, Progress in Oceanography, 91, 167–216, https://doi.org/10.1016/j.pocean.2011.01.002, 2011.

Chenillat, F., Franks, P. J. S., Rivière, P., Capet, X., Grima, N., and Blanke, B.: Plankton dynamics in a cyclonic eddy in the Southern California Current System, Journal of Geophysical Research: Oceans, 120, 5566–5588, https://doi.org/10.1002/2015JC010826, 2015.

Chenillat, F., Deshaies, E., Arens, A., and Penven, P.: Role of mesoscale eddies in the biogeochemistry of the Mozambique Channel, Frontiers in Marine Science, 11, 1402 776, https://doi.org/10.3389/fmars.2024.1402776, 2024.

Cornec, M., Laxenaire, R., Speich, S., and Claustre, H.: Impact of Mesoscale Eddies on Deep Chlorophyll Maxima, Geophysical Research Letters, 48, e2021GL093 470, https://doi.org/10.1029/2021GL093470, e2021GL093470 2021GL093470, 2021.

Cotroneo, Y., Aulicino, G., Ruiz, S., Pascual, A., Budillon, G., Fusco, G., and Tintoré, J.: Glider and satellite high resolution monitoring of a mesoscale eddy in the algerian basin: Effects on the mixed layer depth and biochemistry, Journal of Marine Systems, 162, 73–88, https://doi.org/10.1016/j.jmarsys.2015.12.004, progress in marine science supported by European joint coastal observation systems: The JERICO-RI research infrastructure, 2016.

Crombet, Y., Leblanc, K., Quéguiner, B., Moutin, T., Rimmelin, P., Ras, J., Claustre, H., Leblond, N., Oriol, L., and Pujo-Pay, M.: Deep silicon maxima in the stratified oligotrophic Mediterranean Sea, Biogeosciences, 8, 459–475, https://doi.org/10.5194/bg-8-459-2011, 2011.

Crombie, D. D.: Doppler Spectrum of Sea Echo at 13.56 Mc./s., Nature, 175, 681–682, https://doi.org/10.1038/175681a0, 1955.

Crusius, J., Schroth, A. W., Resing, J. A., Cullen, J., and Campbell, R. W.: Seasonal and spatial variabilities in northern Gulf of Alaska surface water iron concentrations driven by shelf sediment resuspension, glacial meltwater, a Yakutat eddy, and dust, Global Biogeochemical Cycles, 31, 942–960, https://doi.org/10.1002/2016GB005493, 2017.

D'Ortenzio, F., Iudicone, D., de Boyer Montegut, C., Testor, P., Antoine, D., Marullo, S., Santoleri, R., and Madec, G.: Seasonal variability of the mixed layer depth in the Mediterranean Sea as derived from in situ profiles, Geophysical Research Letters, 32, https://doi.org/10.1029/2005GL022463, 2005.

Dufau, C., Orsztynowicz, M., Dibarboure, G., Morrow, R., and Le Traon, P.-Y.: Mesoscale resolution capability of altimetry: Present and future, Journal of Geophysical Research: Oceans, 121, 4910–4927, https://doi.org/10.1002/2015JC010904, 2016.

Ediger, D. and Yilmaz, A.: Characteristics of deep chlorphyll maximum in the Northeastern Mediterranean with respect to environmental conditions, Journal of Marine Systems, 9, 291–303, https://doi.org/10.1016/S0924-7963(96)00044-9, 1996.

Efrati, S., Lehahn, Y., Rahav, E., Kress, N., Herut, B., Gertman, I., Goldman, R., Ozer, T., Lazar, M., and Heifetz, E.: Intrusion of coastal waters into the pelagic eastern Mediterranean: in situ and satellite-based characterization, Biogeosciences, 10, 3349–3357, https://doi.org/10.5194/bg-10-3349-2013, 2013.

El-Rayis, O. and Abdallah, M.: Contribution of Nutrients and some Trace Metals from a Huge Egyptian Drain to the SE-Mediterranean Sea, west of Alexandria, Mediterranean Marine Science, 7, 79–86, https://doi.org/10.12681/mms.179, 2006.

Espinosa-Carreón, T. L., Gaxiola-Castro, G., Beier, E. J., Strub, P. T., and Kurczyn, J. A.: Effects of mesoscale processes on phytoplankton chlorophyll off Baja California, Journal of Geophysical Research, 117, https://api.semanticscholar.org/CorpusID:129296456, 2012.

Estournel, C., Marsaleix, P., and Ulses, C.: A new assessment of the circulation of Atlantic and Intermediate Waters in the Eastern Mediterranean, Progress in Oceanography, 198, 102 673, https://doi.org/10.1016/j.pocean.2021.102673, 2021.

Estrada, M.: Primary production in the northwestern Mediterranean, 1996.

Fadida, Y., Verma, V., Barkan, R., Biton, E., Solodoch, A., and Lehahn, Y.: Coastal-to-offshore submesoscale horizontal stirring enhances wintertime phytoplankton blooms in the ultra-oligotrophic Eastern Mediterranean Sea, Ocean Science, 22, 329–343, https://doi.org/10.5194/os-22-329-2026, 2026.

Fanelli, C., Gomiz Pascual, J. J., Bruno-Mejías, M., and Navarro, G.: Using a Combination of High-Frequency Coastal Radar Dataset and Satellite Imagery to Study the Patterns Involved in the Coastal Countercurrent Events in the Gulf of Cadiz, Remote Sensing, 16, https://doi.org/10.3390/rs16040687, 2024.

Feng, M.: Eddy-induced cross-shelf phytoplankton transport along the downwelling coast off Western Australia, Journal of Tropical Oceanography, pp. 6–10, https://api.semanticscholar.org/CorpusID:129380842, 2009.

Flos, J. and Tintoré, J.: Summer frontal contribution to the fertilization of oceanic waters off the northeast coast of Spain, 1990.

Gerin, R., Poulain, P.-M., Taupier-Letage, I., Millot, C., Ben Ismail, S., and Sammari, C.: Surface circulation in the Eastern Mediterranean using drifters (2005–2007), Ocean Science, 5, 559–574, https://doi.org/10.5194/os-5-559-2009, 2009.

Gertman, I., Goldman, R., Rosentraub, Z., Ozer, T., Zodiatis, G., Hayes, D., and Poulain, P.: Generation of Shikmona anticyclonic eddy from an alongshore current, in: Rapp. Comm. int. Mer Medit.(CIESM Congress Proceedings), vol. 39, p. 114, 2010.

Goldsmith, S., Krom, M., Sandler, A., and Herut, B.: Spatial trends in the chemical composition of sediments on the continental shelf and slope off the Mediterranean coast of Israel, Continental Shelf Research, 21, 1879–1900, https://doi.org/10.1016/S0278-4343(01)00027-9, 2001.

Gurgel, K.-W., Antonischki, G., Essen, H.-H., and Schlick, T.: Wellen Radar (WERA): a new ground-wave HF radar for ocean remote sensing, Coastal Engineering, 37, 219–234, https://doi.org/10.1016/S0378-3839(99)00027-7, 1999.

Gurgel, K.-W., Essen, H.-H., and Schlick, T.: An Empirical Method to Derive Ocean Waves From Second-Order Bragg Scattering: Prospects and Limitations, Oceanic Engineering, IEEE Journal of, 31, 804 – 811, https://doi.org/10.1109/JOE.2006.886225, 2006.

Han, A., Dai, M., Kao, S.-J., Gan, J., Li, Q., Wang, L., Zhai, W., and Wang, L.: Nutrient dynamics and biological consumption in a large continental shelf system under the influence of both a river plume and coastal upwelling, Limnology and Oceanography, 57, 486–502, https://doi.org/10.4319/lo.2012.57.2.0486, 2012.

Hasselmann, K.: Determination of Ocean Wave Spectra from Doppler Radio Return from the Sea Surface, Nature Physical Science, 229, 16–17, https://doi.org/10.1038/physci229016a0, 1971.

Herut, B., Krom, M. D., Pan, G., and Mortimer, R.: Atmospheric input of nitrogen and phosphorus to the Southeast Mediterranean: Sources, fluxes, and possible impact, Limnology and Oceanography, 44, 1683–1692, https://doi.org/10.4319/lo.1999.44.7.1683, 1999.

Herut, B., ALMOGI-LABIN, A., JANNINK, N., and GERTMAN, I.: The seasonal dynamics of nutrient and chlorophyll a concentrations on the SE Mediterranean shelf-slope, Oceanologica Acta, 23, 771–782, https://doi.org/10.1016/S0399-1784(00)01118-X, 2000.

Holte, J., Straneo, F., Moffat, C., Weller, R., and Farrar, J. T.: Structure and surface properties of eddies in the southeast Pacific Ocean, Journal of Geophysical Research: Oceans, 118, 2295–2309, https://doi.org/10.1002/jgrc.20175, 2013.

Ignatiades, L., Gotsis-Skretas, O., Pagou, K., and Krasakopoulou, E.: Diversification of phytoplankton community structure and related parameters along a large east-west transect of the Mediterranean Sea, J. Plankton Res., 31, https://doi.org/10.1093/plankt/fbn124, 2009.

Katz, T., Weinstein, Y., Alkalay, R., Biton, E., Toledo, Y., Lazar, A., Zlatkin, O., Soffer, R., Rahav, E., Sisma-Ventura, G., Bar, T., Ozer, T., Gildor, H., Almogi-Labin, A., Kanari, M., Berman-Frank, I., and Herut, B.: The first deep-sea mooring station in the eastern Levantine basin (DeepLev), outline and insights into regional sedimentological processes, Deep Sea Research Part II: Topical Studies in Oceanography, 171, 104 663, https://doi.org/10.1016/j.dsr2.2019.104663, revisiting the Eastern Mediterranean: Recent knowledge on the physical, biogeochemical and ecosystemic states and trends (Volume II), 2020.

Kress, N. and Herut, B.: Hypernutrification in the Oligotrophic Eastern Mediterranean: a Study in Haifa Bay (Israel), Estuarine, Coastal and Shelf Science, 46, 645–656, https://doi.org/10.1006/ecss.1997.0302, 1998.

Kress, N. and Herut, B.: Spatial and seasonal evolution of dissolved oxygen and nutrients in the Southern Levantine Basin (Eastern Mediterranean Sea): chemical characterization of the water masses and inferences on the N:P ratios, Deep Sea Research Part I: Oceanographic Research Papers, 48, 2347–2372, https://doi.org/10.1016/S0967-0637(01)00022-X, 2001.

Krom, M., Brenner, S., Kress, N., Neori, A., and Gordon, L.: Nutrient dynamics and new production in a warm-core eddy from the Eastern Mediterranean Sea, Deep Sea Research Part A. Oceanographic Research Papers, 39, 467–480, https://doi.org/10.1016/0198-0149(92)90083-6, 1992.

Krom, M., Woodward, E., Herut, B., Kress, N., Carbo, P., Mantoura, R., Spyres, G., Thingstad, T., Wassmann, P., Wexels-Riser, C., Kitidis, V., Law, C., and Zodiatis, G.: Nutrient cycling in the south east Levantine basin of the eastern Mediterranean: Results from a phosphorus starved system, Deep Sea Research Part II: Topical Studies in Oceanography, 52, 2879–2896, https://doi.org/10.1016/j.dsr2.2005.08.009, on the Nature of Phosphorus Cycling and Limitation in the Eastern Mediterranean, 2005.

Krom, M., Emeis, K.-C., and Van Cappellen, P.: Why is the Eastern Mediterranean phosphorus limited?, Progress in Oceanography, 85, 236–244, https://doi.org/10.1016/j.pocean.2010.03.003, 2010.

Krom, M., Kress, N., Berman-Frank, I., and Rahav, E.: Past, Present and Future Patterns in the Nutrient Chemistry of the Eastern Mediterranean, pp. 49–68, Springer Netherlands, Dordrecht, https://doi.org/10.1007/978-94-007-6704-1_4, 2014.

Krom, M. D., Herut, B., and Mantoura, R. F. C.: Nutrient budget for the Eastern Mediterranean: Implications for phosphorus limitation, Limnology and Oceanography, 49, 1582–1592, https://doi.org/10.4319/lo.2004.49.5.1582, 2004.

Kurkin, A., Kurkina, O., Rybin, A., and Talipova, T.: Comparative analysis of the first baroclinic Rossby radius in the Baltic, Black, Okhotsk, and Mediterranean seas, Russian Journal of Earth Sciences, 20, –, 2020.

Levy, M., Klein, P., and Treguier, A.-M.: Impact of sub-mesoscale physics on production and subduction of phytoplankton in an oligotrophic regime, Journal of Marine Research, 59, 535–565, https://archimer.ifremer.fr/doc/00000/800/, 2001.

Lévy, M., Franks, P. J. S., and Smith, K. S.: The role of submesoscale currents in structuring marine ecosystems, Nature Communications, 9, 4758, https://doi.org/10.1038/s41467-018-07059-3, 2018.

Li, Q. P., Hansell, D. A., McGillicuddy Jr., D. J., Bates, N. R., and Johnson, R. J.: Tracer-based assessment of the origin and biogeochemical transformation of a cyclonic eddy in the Sargasso Sea, Journal of Geophysical Research: Oceans, 113, https://doi.org/10.1029/2008JC004840, 2008.

Lorente, P., Aguiar, E., Bendoni, M., Berta, M., Brandini, C., Cáceres-Euse, A., Capodici, F., Cianelli, D., Ciraolo, G., Corgnati, L., Dadić, V., Doronzo, B., Drago, A., Dumas, D., Falco, P., Fattorini, M., Gauci, A., Gómez, R., Griffa, A., Guérin, C.-A., Hernández-Carrasco, I., Hernández-Lasheras, J., Ličer, M., Magaldi, M. G., Mantovani, C., Mihanović, H., Molcard, A., Mourre, B., Orfila, A., Révelard, A., Reyes, E., Sánchez, J., Saviano, S., Sciascia, R., Taddei, S., Tintoré, J., Toledo, Y., Ursella, L., Uttieri, M., Vilibić, I., Zambianchi, E., and

Cardin, V.: Coastal high-frequency radars in the Mediterranean – Part 1: Status of operations and a framework for future development, Ocean Science, 18, 761–795, https://doi.org/10.5194/os-18-761-2022, 2022.

Lévy, M., Ferrari, R., Franks, P. J. S., Martin, A. P., and Rivière, P.: Bringing physics to life at the submesoscale, Geophysical Research Letters, 39, https://doi.org/10.1029/2012GL052756, 2012.

Malan, N., Roughan, M., Hemming, M., and Schaeffer, A.: Mesoscale Circulation Controls Chlorophyll Concentrations in the East Australian Current Separation Zone, Journal of Geophysical Research: Oceans, 128, e2022JC019 361, https://doi.org/10.1029/2022JC019361, 2023.

Martin, A.: Phytoplankton patchiness: The role of lateral stirring and mixing, Progress In Oceanography, 57, 125–174, https://doi.org/10.1016/S0079-6611(03)00085-5, 2003.

Marullo, S., Napolitano, E., Santoleri, R., Manca, B., and Evans, R.: Variability of Rhodes and Ierapetra Gyres during Levantine Intermediate Water Experiment: Observations and model results, Journal of Geophysical Research: Oceans, 108, 8119, https://doi.org/10.1029/2002JC001393, 2003.

McNeil, J. D., Jannasch, H. W., Dickey, T., McGillicuddy, D., Brzezinski, M., and Sakamoto, C. M.: New chemical, bio-optical and physical observations of upper ocean response to the passage of a mesoscale eddy off Bermuda, Journal of Geophysical Research: Oceans, 104, 15 537–15 548, https://doi.org/10.1029/1999JC900137, 1999.

Menna, M., Poulain, P.-M., Zodiatis, G., and Gertman, I.: On the surface circulation of the Levantine sub-basin derived from Lagrangian drifters and satellite altimetry data, Deep Sea Research Part I: Oceanographic Research Papers, 65, 46–58, https://doi.org/10.1016/j.dsr.2012.02.008, 2012.

Mignot, A., Claustre, H., Uitz, J., Poteau, A., D'Ortenzio, F., and Xing, X.: Understanding the seasonal dynamics of phytoplankton biomass and the deep chlorophyll maximum in oligotrophic environments: A Bio-Argo float investigation, Global Biogeochemical Cycles, 28, 856–876, https://doi.org/10.1002/2013GB004781, 2014.

Moore, T. S., Matear, R. J., Marra, J., and Clementson, L.: Phytoplankton variability off the Western Australian Coast: Mesoscale eddies and their role in cross-shelf exchange, Deep Sea Research Part II: Topical Studies in Oceanography, 54, 943–960, https://doi.org/10.1016/j.dsr2.2007.02.006, 2007.

Morel, A. and Maritorena, S.: Bio-optical properties of oceanic waters: A reappraisal, Journal of Geophysical Research: Oceans, 106, 7163–7180, https://doi.org/10.1029/2000JC000319, 2001.

Moutin, T., Van Wambeke, F., and Prieur, L.: Introduction to the Biogeochemistry from the Oligotrophic to the Ultraoligotrophic Mediterranean (BOUM) experiment, Biogeosciences, 9, 3817–3825, https://doi.org/10.5194/bg-9-3817-2012, 2012.

Navarro, G. and Ruiz, J.: Spatial and temporal variability of phytoplankton in the Gulf of Cádiz through remote sensing images, Deep Sea Research Part II: Topical Studies in Oceanography, 53, 1241–1260, https://doi.org/10.1016/j.dsr2.2006.04.014, 2006.

Neukermans, G., Reynolds, R., and Stramski, D.: Contrasting inherent optical properties and particle characteristics between an under-ice phytoplankton bloom and open water in the Chukchi Sea, Deep Sea Research Part II: Topical Studies in Oceanography, 105, https://doi.org/10.1016/j.dsr2.2014.03.014, 2014.

Nixon, S. W.: Replacing the Nile: Are anthropogenic nutrients providing the fertility once brought to the Mediterranean by a great river?, Ambio, 32, 30–39, https://doi.org/10.1579/0044-7447-32.1.30, 2003.

Oczkowski, A. J., Nixon, S. W., Granger, S. L., El-Sayed, A.-F. M., and McKinney, R. A.: Anthropogenic enhancement of Egypt's Mediterranean fishery, Proceedings of the National Academy of Sciences, 106, 1364–1367, https://doi.org/10.1073/pnas.0812568106, 2009.

Ozer, T., Gertman, I., Kress, N., Silverman, J., and Herut, B.: Interannual thermohaline (1979–2014) and nutrient (2002–2014) dynamics in the Levantine surface and intermediate water masses, SE Mediterranean Sea, Global and Planetary Change, 151, 60–67, https://doi.org/10.1016/j.gloplacha.2016.04.001, climate Variability and Change in the Mediterranean Region, 2017.

Ozer, T., Gertman, I., Gildor, H., and Herut, B.: Thermohaline Temporal Variability of the SE Mediterranean Coastal Waters (Israel) – Long-Term Trends, Seasonality, and Connectivity, Frontiers in Marine Science, 8, https://doi.org/10.3389/fmars.2021.799457, 2022.

Paulino, A., Heldal, M., Norland, S., and Egge, J.: Elemental stoichiometry of marine particulate matter measured by wavelength dispersive X-ray fluorescence (WDXRF) spectroscopy, Journal of the Marine Biological Association of the United Kingdom, 93, 2003–2014, https://doi.org/10.1017/S0025315413000635, 2013.

Pegliasco, C., Chaigneau, A., Morrow, R., and Dumas, F.: Detection and tracking of mesoscale eddies in the Mediterranean Sea: A comparison between the Sea Level Anomaly and the Absolute Dynamic Topography fields, Advances in Space Research, 68, 401–419, https://doi.org/10.1016/j.asr.2020.03.039, 25 Years of Progress in Radar Altimetry, 2021.

Pessini, F., Olita, A., Cotroneo, Y., and Perilli, A.: Mesoscale eddies in the Algerian Basin: do they differ as a function of their formation site?, Ocean Science, 14, 669–688, https://doi.org/10.5194/os-14-669-2018, 2018.

Pessini, F., Cotroneo, Y., Olita, A., Sorgente, R., Ribotti, A., Jendersie, S., and Perilli, A.: Life history of an anticyclonic eddy in the Algerian basin from altimetry data, tracking algorithm and in situ observations., Journal of Marine Systems, 207, 103 346, https://doi.org/10.1016/j.jmarsys.2020.103346, 2020.

Poulain, P.-M., Bussani, A., Gerin, R., Jungwirth, R., Menna, M., and Notarstefano, G.: Mediterranean Surface Currents Measured with Drifters: From Basin to Subinertial Scales, Oceanography, 26, 38–47, https://doi.org/10.5670/oceanog.2013.03, 2013.

Poulain, P.-M., Centurioni, L., Özgökmen, T., Tarry, D., Pascual, A., Ruiz, S., Mauri, E., Menna, M., and Notarstefano, G.: On the Structure and Kinematics of an Algerian Eddy in the Southwestern Mediterranean Sea, Remote Sensing, 13, https://doi.org/10.3390/rs13153039, 2021.

Powley, H. R., Krom, M. D., and Van Cappellen, P.: Understanding the unique biogeochemistry of the Mediterranean Sea: Insights from a coupled phosphorus and nitrogen model, Global Biogeochemical Cycles, 31, 1010–1031, https://doi.org/10.1002/2017GB005648, 2017.

Psarra, S., Tselepides, A., and Ignatiades, L.: Primary productivity in the oligotrophic Cretan Sea (NE Mediterranean): seasonal and interannual variability, Progress in Oceanography, 46, 187–204, https://doi.org/10.1016/S0079-6611(00)00018-5, 2000.

Pujo-Pay, M., Conan, P., Oriol, L., Cornet-Barthaux, V., Falco, C., Ghiglione, J.-F., Goyet, C., Moutin, T., and Prieur, L.: Integrated survey of elemental stoichiometry (C, N, P) from the western to eastern Mediterranean Sea, Biogeosciences, 8, 883–899, https://doi.org/10.5194/bg-8-883-2011, 2011.

Raveh, O., David, N., Rilov, G., and Rahav, E.: The Temporal Dynamics of Coastal Phytoplankton and Bacterioplankton in the Eastern Mediterranean Sea, PLOS ONE, 10, 1–23, https://doi.org/10.1371/journal.pone.0140690, 2015.

Reich, T., Ben-Ezra, T., Belkin, N., Tsemel, A., Aharonovich, D., Roth-Rosenberg, D., Givati, S., Bialik, M., Herut, B., Berman-Frank, I., Frada, M., Krom, M. D., Lehahn, Y., Rahav, E., and Sher, D.: A year in the life of the Eastern Mediterranean: Monthly dynamics of phytoplankton and bacterioplankton in an ultra-oligotrophic sea, Deep Sea Research Part I: Oceanographic Research Papers, 182, 103 720, https://doi.org/10.1016/j.dsr.2022.103720, 2022.

Ribera d'Alcalà, M., Civitarese, G., Conversano, F., and Lavezza, R.: Nutrient ratios and fluxes hint at overlooked processes in the Mediterranean Sea, Journal of Geophysical Research: Oceans, 108, https://doi.org/10.1029/2002JC001650, 2003.

Robinson, A., Golnaraghi, M., Leslie, W., Artegiani, A., Hecht, A., Lazzoni, E., Michelato, A., Sansone, E., Theocharis, A., and Unluata, U.: The eastern Mediterranean general circulation: features, structure and variability, Dynamics of Atmospheres and Oceans, 15, 215–240, https://doi.org/10.1016/0377-0265(91)90021-7, the Mediterranean Sea, 1991.

Robinson, A. R., Leslie, W. G., Theocharis, A., and Lascaratos, A.: Mediterranean Sea Circulation, in: Encyclopedia of Ocean Sciences, edited by Steele, J. H., Thorpe, S. A., and Turekian, K. K., pp. 1689–1705, Academic Press, https://doi.org/10.1006/rwos.2001.0376, 2001.

Rosentraub, Z. and Brenner, S.: Circulation over the southeastern continental shelf and slope of the Mediterranean Sea: Direct current measurements, winds, and numerical model simulations, Journal of Geophysical Research: Oceans, 112, https://doi.org/10.1029/2006jc003775, 2007.

Rubin-Blum, M., Sisma-Ventura, G., Yudkovski, Y., Belkin, N., Kanari, M., Herut, B., and Rahav, E.: Diversity, activity, and abundance of benthic microbes in the Southeastern Mediterranean Sea, FEMS Microbiology Ecology, 98, fiac009, https://doi.org/10.1093/femsec/fiac009, 2022.

Rubio, A., Caballero, A., Orfila, A., Hernández-Carrasco, I., Ferrer, L., González, M., Solabarrieta, L., and Mader, J.: Eddy-induced cross-shelf export of high Chl-a coastal waters in the SE Bay of Biscay, Remote Sensing of Environment, 205, 290–304, https://doi.org/10.1016/j.rse.2017.10.037, 2018.

Siokou-Frangou, I., Christaki, U., Mazzocchi, M. G., Montresor, M., Ribera d'Alcalá, M., Vaqué, D., and Zingone, A.: Plankton in the open Mediterranean Sea: a review, Biogeosciences, 7, 1543–1586, https://doi.org/10.5194/bg-7-1543-2010, 2010.

Solidoro, C., Bastianini, M., Bandelj, V., Codermatz, R., Cossarini, G., Melaku Canu, D., Ravagnan, E., Salon, S., and Trevisani, S.: Current state, scales of variability, and trends of biogeochemical properties in the northern Adriatic Sea, Journal of Geophysical Research: Oceans, 114, https://doi.org/10.1029/2008JC004838, 2009.

Solodoch, A., Barkan, R., Verma, V., Gildor, H., Toledo, Y., Khain, P., and Levi, Y.: Basin-Scale to Submesoscale Variability of the East Mediterranean Sea Upper Circulation, Journal of Physical Oceanography, 53, 2137 – 2158, https://doi.org/10.1175/JPO-D-22-0243.1, 2023.

Sutyrin, G., Stegner, A., Taupier-Letage, I., and Teinturier, S.: Amplification of a Surface-Intensified Eddy Drift along a Steep Shelf in the Eastern Mediterranean Sea, Journal of Physical Oceanography, 39, 1729 – 1741, https://doi.org/10.1175/2009JPO4106.1, 2009.

Teruzzi, A., Bolzon, G., Feudale, L., and Cossarini, G.: Deep chlorophyll maximum and nutricline in the Mediterranean Sea: emerging properties from a multi-platform assimilated biogeochemical model experiment, Biogeosciences, 18, 6147–6166, https://doi.org/10.5194/bg-18-6147-2021, 2021.

van Leeuwen, S. M., Beecham, J. A., García-García, L. M., and Thorpe, R.: The Mediterranean Rhodes Gyre: modelled impacts of climate change, acidification and fishing, Marine Ecology Progress Series, 690, pp. 31–50, https://www.jstor.org/stable/27179442, 2022.

Verma, V., Barkan, R., Solodoch, A., Gildor, H., and Toledo, Y.: The Eastern Mediterranean Boundary Current: Seasonality, Stability, and Spiral Formation, Journal of Physical Oceanography, 54, 1971–1989, https://doi.org/10.1175/jpo-d-23-0207.1, 2024.

Volpe, G., Buongiorno Nardelli, B., Colella, S., Pisano, A., and Santoleri, R.: An Operational Interpolated Ocean Colour Product in the Mediterranean Sea, https://doi.org/10.17125/gov2018.ch09, 2018.

Volpe, G., Colella, S., Brando, V., Forneris, V., Padula, F., Di Cicco, A., Sammartino, M., Bracaglia, M., Artuso, F., and Santoleri, R.: The Mediterranean Ocean Colour Level 3 Operational Multi-Sensor Processing, Ocean Science Discussions, pp. 1–26, https://doi.org/10.5194/os-2018-73, 2019.

Wang, Y., Zhang, H.-R., Chai, F., and Yuan, Y.: Impact of mesoscale eddies on chlorophyll variability off the coast of Chile, PLOS ONE, 13, 1–13, https://doi.org/10.1371/journal.pone.0203598, 2018.

Washburn, L., Swenson, M. S., Largier, J. L., Kosro, P. M., and Ramp, S. R.: Cross-Shelf Sediment Transport by an Anticyclonic Eddy Off Northern California, Science, 261, 1560–1564, https://doi.org/10.1126/science.261.5128.1560, 1993.

Wyatt, L.: High-frequency radar measurements of the ocean wave-directional spectrum, IEEE Journal of Oceanic Engineering, 16, 163–169, https://doi.org/10.1109/48.64896, 1991.

Xu, W., Wang, G., Cheng, X., Xing, X., Qin, J., Zhou, G., Jiang, L., and Chen, B.: Mesoscale Eddy Modulation of Subsurface Chlorophyll Maximum Layers in the South China Sea, Journal of Geophysical Research: Biogeosciences, 128, e2023JG007 648, https://doi.org/10.1029/2023JG007648, e2023JG007648 2023JG007648, 2023.

Zeng, L. and Li, D.: Development of In Situ Sensors for Chlorophyll Concentration Measurement, Journal of Sensors, 2015, 903 509, https://doi.org/10.1155/2015/903509, 2015.

Zodiatis, G., Brenner, S., Gertman, I., Ozer, T., Simoncelli, S., Ioannou, M., and Savva, S.: Twenty years of in-situ monitoring in the south-eastern Mediterranean Levantine basin: Basic elements of the thermohaline structure and of the mesoscale circulation during 1995-2015, Frontiers in Marine Science, 9, https://doi.org/10.3389/fmars.2022.1074504, 2023.

Zohary, T. and Robarts, R. D.: Experimental study of microbial P limitation in the eastern Mediterranean, Limnology and Oceanography, 43, 387–395, https://doi.org/10.4319/lo.1998.43.3.0387, 1998.